Summer 2024

Production of Glass-To-Metal Seals using Additive Manufacturing Techniques

Aaron Read
Missouri University of Science and Technology

Department:

PRODUCTION OF GLASS-TO-METAL SEALS USING ADDITIVE MANUFACTURING TECHNIQUES

by

AARON REECE READ

A THESIS

Presented to the Graduate Faculty of the

MISSOURI UNIVERSITY OF SCIENCE AND TECHNOLOGY

In Partial Fulfillment of the Requirements for the Degree

MASTER OF SCIENCE IN MATERIALS SCIENCE AND ENGINEERING

2023

Approved by:

Richard Brow, Advisor
Douglas Bristow
F. Scott Miller

PUBLICATION THESIS OPTION

This thesis consists of the following two articles, formatted in the style used by the Missouri University of Science and Technology:

Paper I: Pages 13-39 are intended for submission to International Journal of Applied Glass Science

Paper II: Pages 40-64 are intended for submission to International Journal of Applied Glass Science

ABSTRACT

Glass-to-metal (GtM) seals are hermetic barriers between glass and metal components, often used in the electronic and vacuum industries. Creating the seals traditionally requires heating all the components to the glass melting temperature, where the glass will flow and bond to the metal. Due to the manufacturing constraints of the individual components and sealing conditions there are geometric and material restrictions. Additive manufacturing techniques were used to make GtM seals to reduce these restrictions.

Hermetic, single pin seals were produced using printed metal shells, by selective laser melting (SLM), and digital light processing (DLP) printed glass preforms. Glass preforms were printed with photosensitive resin mixed with a silicate sealing glass powder in a 1:2 weight ratio. Thermal analysis, TGA/DSC, and screening experiments were used to determine an organic removal schedule. Video techniques determined a sintering schedule by producing a densification curve at different isothermal holds which were fit with a viscous sintering model.

Single pin seals were also produced use a laser assisted manufacturing (LAM) process as an alternative to the conventional furnace sealing process. A Nd:YAG laser was focused on a solid glass preform, heating the glass to form the glass-metal bond. The sealing glass was doped with a transition metal oxide, Fe_2O_3 or CuO, to increase absorption of the laser wavelength. The interface of hermetic LAM seals were analyzed using electron microscopy, compared to conventional prepared seals, finding a reduction of interfacial morphologies.

ACKNOWLEDGMENTS

This work is funded by the Department of Energy's Kansas City National Security Campus, operated by Honeywell Federal Manufacturing & Technologies, LLC, under contract number DE-NA0002839

Firstly, I would like to extend my gratitude to Kansas City National Security Campus (KCNSC) for providing funding and direction for this project. Special thanks to the people who have managed this project from KCNSC including Rachel Grodsky, Dennis Eichorst, and Parker Freudenberger.

I would like to thank my advisor Dr. Richard Brow for hiring me for this position and then providing encouragement, taking time to answer our endless questions, and most of all helping edit this paper.

Many thanks to the Advance Materials Characterization Lab (AMCL) and Material Research Center (MRC) at Missouri S&T for allowing me to use their equipment to further this research, and to Patty and Sissy keeping everything afloat. A very special thanks to Fred Eichelmann for letting me use his machining equipment and being there to fix all the problems we threw at him, and they were numerous.

Finally, and definitely not least, I would like to thank my family, friends, and colleagues. Thanks to my amazing undergraduate research assistants Makayla, Will, and Grace for helping this project progress as far as it has. To my fellow graduate students, especially Noah and Sydney for dealing with me daily. And to my Parents, Ted and Diane, and brother, Daniel, for being there for me whether it was asked for help or not.

"It takes a village"

TABLE OF CONTENTS

Page

LIST OF ILLUSTRATIONS

SECTION Page

PAPER II

LIST OF TABLES

PAPER I Page

PAPER II

NOMENCLATURE

Symbol	Description
η	Viscosity
L	Uniaxial load
h	Hieght
V	Volume
ρ_s	Density of sample
ρ_m	Density of buoyancy fluid
w_a	Mass of sample in air
w_b	Mass of sample in buoyancy fluid
η_∞	Viscosity at infinitely high temperature
T_g	Glass transition temperature
T_g	Temperature
m	Fragility
ρ_o	Initial density
ρ_g	Density of bulk glass
γ	Surface energy
t	Time
r	Radius of particle

$a_o(r)$	Average pore size
$\theta(t_{0.8} - t)$	Step function for times before 0.8 relative density
$\theta(t - t_{0.8})$	Step function for times after 0.8 relative density
q"	Heat flux
α	Absorptivity
P	Laser Power
r_o	Laser waist diameter
R	Distance from beam center
ΔG	Gibb's free energy

SECTION

1. INTRODUCTION

1.1. BACKGROUND

Glass-to-metal (GtM) seals traditionally are formed through melting glass and bonding to a metal surface. This creates a hermetic barrier between the glass and metal components. These seals can be used for a wide range of applications, notably Eddison used a GtM seal to make the incandescent light bulb.[1] The usefulness of seals persists with most modern applications for this technology being in the electrical and vacuum connecters industries. The mechanisms to create seals have been extensively studied showing certain material combinations are ideal, while other glass-metal combinations should be avoided.[1-5] The restriction of materials is due to thermal-chemical compatibility between the glass and metal with current processing techniques.[2-5] New processing techniques to create a glass-to-metal seal could be implemented to open a larger catalog of material combinations and applications.

The following introduction reviews information on glass-to-metal seals and additive manufacturing of sealing materials.

1.2. GLASS-TO-METAL SEALS

Seals are often composed of three major components: A metal shell, metal pin, and a glass preform. Seals can be various sizes and shapes depending on application, different types of seals shown in Figure 1.1.[6]

Figure 1.1: Different types of glass-to-metal seals showing variation in size and shapes of the electrical connector by Complete Hermetic.[6]

Seals are formed through a thermal process of heating up the assembled components to the melting temperature of the glass, around 1000°C.[2] Here the glass will flow and wet to the metal, where oxides from the glass will react to the metal, forming a bond.[1] The seal is then cooled to room temperature where thermal stress are introduced to the system through thermal expansion mismatch in the sample.[2,4]

1.2.1. Seal Component Selection. Glasses are paired with the metal for their thermal and chemical compatibility.[3,4] Often the glass matches thermal properties of the pin, in particular the coefficient of thermal expansion (CTE).[2] Matching the CTE reduces the internal tensile stress of the glass, which generally should not exceed 10 MPa.[7] The CTE of the shell material is also considered and classifies seals into matched seals, shell having the same CTE as the glass, or compression seals, shell having a higher CTE than the glass.[4] Compression seals aid in hermeticity by mechanically reducing any gap between the shell and preform. Different combinations of component expansion properties lead to stresses that may cause various defects in the glass after sealing, illustrated in Figure 1.2. [2]

Figure 1.2: Illustration of possible cracking from thermal stresses with (a-b) showing cracks formed from a compressive seal and (c) if the pin has a higher expansion than the glass adapted from Rulon.[2]

Glass expansion coefficients can be affected by additives in the glass. 40 wt% Fe_2O_3 added to a sodium silicate glass will lower the thermal expansion from $160x10^{-7}/^oC$ to $130x10^{-7}/^oC$ to closer match with an iron substrate.[8] This can work with other glass modifiers for a similar effect.[1]

At the sealing temperature, chemical reactions are possible between oxides in the glass and the metal components.[2,3] The metal will reduce the glass reactant creating an interfacial layer, Figure 1.3a.[3] This layer will grow until meeting the local saturation point, then the interfacial layer will diffuse into the bulk of the glass. The diffusion will continue until ideally there is a mono-atomic oxide bond at the interface, Figure 1.3b.[3] Large interface layers can prove addition stress to the seal if the thermomechanical properties differ to the other sealing materials, leading to a decreased seal lifetime.[9]

This interfacial reaction commonly occur with the alkaline oxides or other easily reduced oxides in the glass.[3,10] The alkaline oxide will be reduced to metal, iron-soda reaction in Equation 1.[3] CoO, NiO, CuO, and other oxides can be added to the glass

promote a chemical reaction at the interface.[1] Here it the oxide is reduce to a lower valence state or to their metallic state.

$$Fe + Na_2O \rightarrow FeO + 2Na_g \quad (1)$$

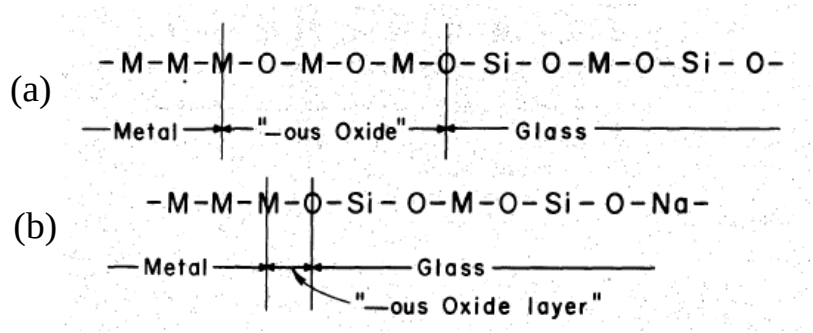

Figure 1.3: Schematic of the glass-metal interface of a seal showing (top, a) a thick interfacial layer and (bottom, b) a mono-atomic interfacial layer found by Pask .[3]

Reactive metals, such as Cr and Ti, will readily form an interfacial layer.[11,12] Due to the slow diffusion of chrome and titanium reactants into the glass, the interfacial layer does not diminish during sintering.[11] This weakens the glass-metal bond at the interface. Cr^{3+} reactants will form a large interfacial layer, Figure 1.4, when pair with a lithium silicate glass.[14] Ti when paired with a lithium silicate will from a Ti_xSi_y phases in addition to TiO_2 at the interface.[12] Due to high relativity a borate glass is often paired with a Ti shell seal.[14]

For a good seal to be formed the stresses created from thermal expansion mismatch and the possible interface layer should not negatively impact bond between the glass and metal. Tensile stress should be avoided, while some compressive stress could aid in hermeticity. This seal should also have a thin, ideally mono-atomic thick, interfacial layer, while oxides in the glass help promote this bond occurring.

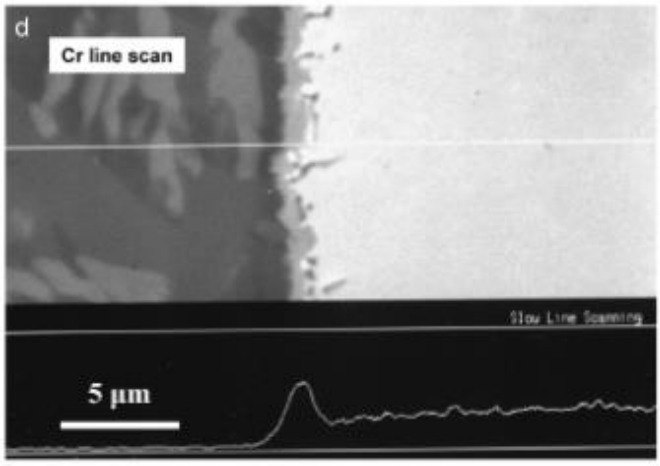

Figure 1.4: Cr EDS line scan showing a high chrome containing interfacial layer between and lithium zinc silicate glass, left of the interface, and Inconel 625, right of the interface, studied by Donald, Metcalfe and Gerrard.[13]

1.2.2. Hermeticity Testing. For most seal applications water or other unwanted atmospheric conditions could lead to catastrophic failure for the product. The hermeticity of a seal is tested through a helium leak test where helium is pass through the seal. The machine will detect the partial pressure of the helium and report it as a pressure-volume per time unit, often atm*cc/sec.[15] Hermetic seals leak rates are generally on the order of $1x10^{-8}$ atm*cc/sec.[2]

1.3. ADDITIVE MANUFACTURING OF SEAL MATERIALS

Additive manufacturing (AM) techniques are methods that produce monolithic structure to the desired dimension and properties without the need to remove material.[16] These processes can take the material and layer-by-layer build the three-dimension structure. This can be done on metal, ceramic, or polymer materials.

1.3.1. Laser Melting of Materials. Selective laser melting (SLM) and Selective laser melting (SLS) are AM methods where a laser is used to melt or sinter a layer of

powder to build a monolithic part.[17,18] Figure 1.5 shows a schematic of the SLM processing method.[19] Material powder is spread over the printing surface where the powder interacts with a laser. The material, absorbing the energy of the laser, heats up. As it approaches half of it melting the powders will start to neck and sinter, for SLS, described more thoroughly in a later section, making a dense piece.[17] For SLM, the laser melts the powder layer that then crystallizes upon cooling.[18] For both methods a new powder layer is then added, and the process repeats until the final monolithic piece is completed. Each new layer is generally around 50 µm thick.[20]

Typically, this is done on metal powders, however, this process could be replicated for other materials that can absorb the laser's energy. Glass has been shown to have success laser processing with both CO_2 and Nd:YAG lasers with a filament fed and powder bed process, respectively.[21,22] The amount of energy transferred is dependent on the absorption of the glass.[21]

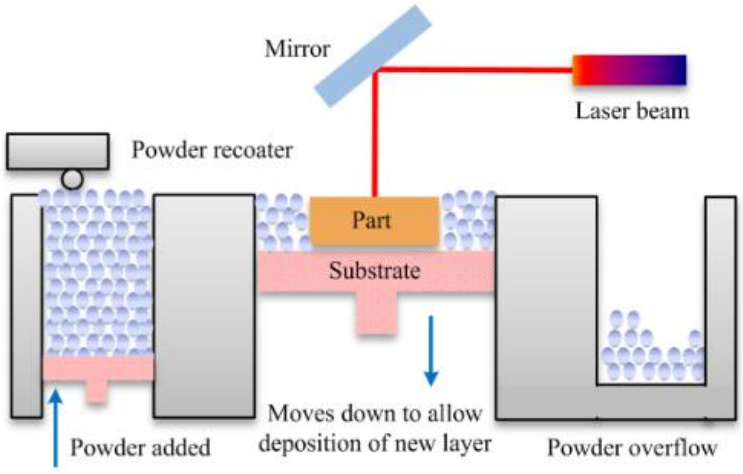

Figure 1.5: Schematic of the selective laser melting (SLM) process shown by Zhang.[19]

Glass absorption in visible, and near-infrared (IR), light can be altered by the used of transition metal oxides.[23] Light absorption occurs through the light energy being

sufficient to excite an electron in the metal ion ligand field.[24] The exited election will transition to higher energy state. Figure 1.6 show example absorption spectra for Fe^{2+}.[25]

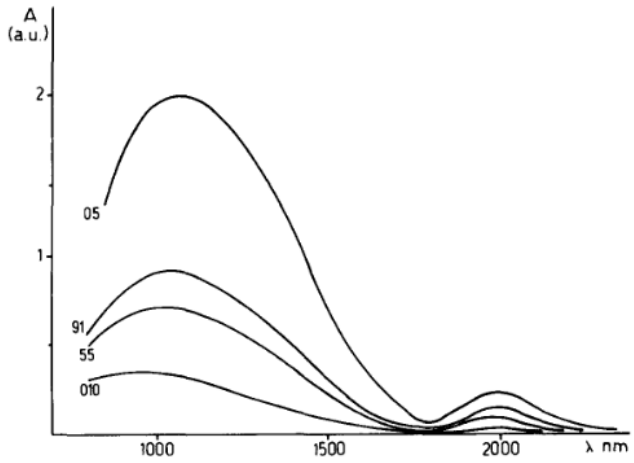

Figure 1.6: Example visible light absorption spectra of soda-lime-silicate glass doped with Fe^{2+} showing a peak absorption around 1000-1100nm adapted by Montenero.[25]

This energy gap can change for different oxidation states of a metal ion. An example is Fe^{2+} has a peak absorption at about 1100 nm in the near IR spectra but Fe^{3+} has a peak absorption near 380 nm near the UV wavelengths.[25,26] This is considered when pairing glasses with a laser where Fe^{2+} will perform well with a near IR laser, such as a ND:YAG laser.

1.3.2. Resin Vat Printing. Vat photopolymerization is a technique that selectively polymerizes resin with an ultraviolet (UV) light source onto a build plate.[27] Digital light processing (DLP) and stereolithography (SLA) are two common types of resin vat printing.[27,28] SLA scans a laser over the resin for polymerization, where DLP focus a larger area of light with the use of a digital micromirror device (DMD). Figure 1.7 shows how SLA, top image, and DLP, bottom image, differ from each other.[27] DLP

focuses ultraviolet (UV) light source using the DMD and cures a whole layer of resin, typically 100 µm thick, simultaneously onto the build plate.[27,29] This repeats layer-by-layer until the print is complete.[27] This makes the DLP process faster than SLA.[27]

The photosensitive resin, typically an acrylate resin, can be printed with a suspended powder that is encapsulated when the resin polymerizes.[27] Different powders can be added to the resin; however, the resin should keep a viscosity less 0.5 Pa*s at the printing temperature.[30] If the encapsulated powder is the final material desired, then the printed piece will have to go through a burnout and sintering step to get a dense part.

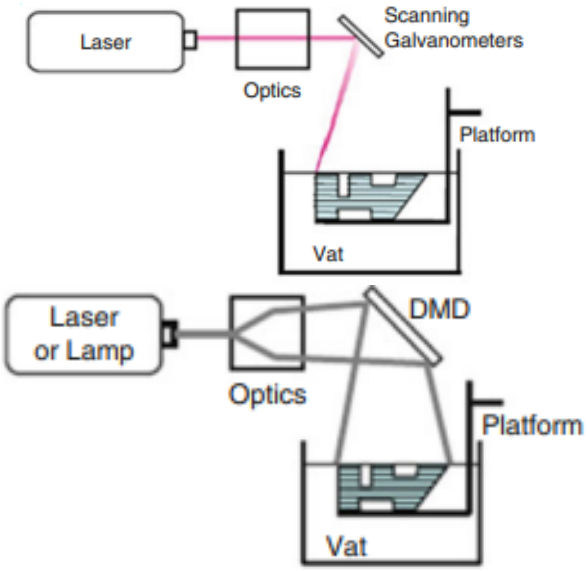

Figure 1.7: Schematic of SLA ,top, and DLP, bottom, processes for resin vat printing processes shown by Gibson.[27]

1.3.2.1. Organic removal. The removal of organics (burnout) of resin-powder pieces occurs in three major stages.[31]The first stage involves slowly heating, typically round 0.17-1°C/min, the piece to the soften temperature of the organics. [32] Too slow of a ramp rate will cause cracking in the sample, while a faster ramp rate will trap organics

gasses later in the burnout process.[31]The stages two and three involve decomposition and evaporation of organics with a slow ramp rate, stage two, or a faster ramp rate, stage three.[33,34] Stage two additionally has organic transport through capillary action throughout the piece.[33] Figure 1.8 shows an example organic burnout schedule.[31]

Depending on the burnout atmosphere, different burnout temperatures and ramp rates are needed. In oxygenating atmospheres, it is possible for the organics to polymerize and crosslink into larger structures that require higher temperature to revome.[35] However, excess oxygen initiates decomposition at lower temperature and removes organics a faster rate.[3]

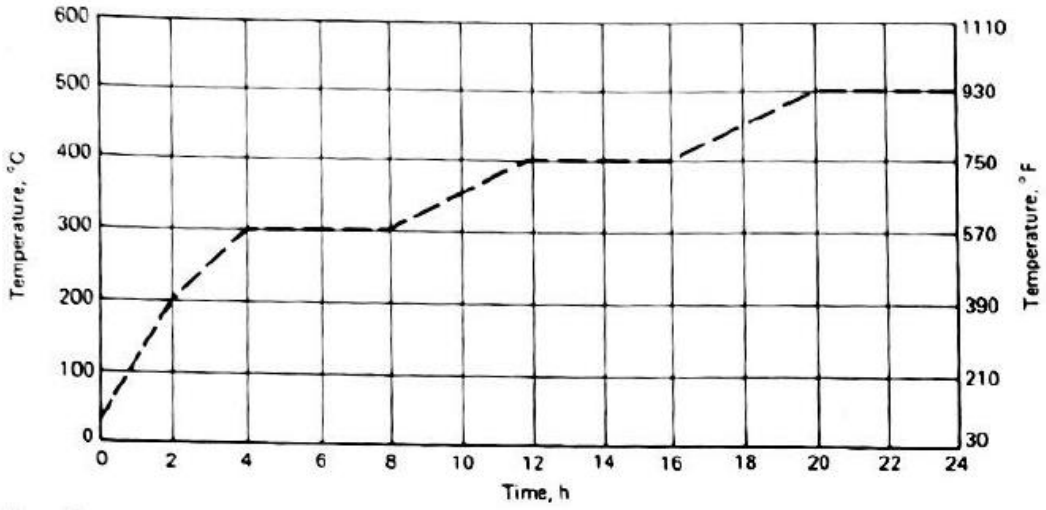

Figure 1.8: Example burnout schedule for an organic burnout adapted from Hermanson.[31]

1.3.2.2. Densification of powders. After the organic burnout the powders must sinter to form a dense piece. Sintering mechanisms can be distributed into two major categories: non-densifying and densifying mechanisms.[36] Both mechanisms involve matter transport to form and grow necks between two or more particles, seen in Figure

1.9.[36] Surface diffusion, lattice diffusion and vapor transport, steps 1-3 in Figure 1.9, are non-densifying, meaning they form and grow necks without increasing the density of the material. Grain boundary diffusion, lattice diffusion, and plastic flow, Steps 4-6 in Figure 1.9, are densification mechanisms with grain boundary diffusion and lattice diffusion being most common for polycrystalline ceramic. Plastic flow mechanism are more common for metals.[17,36]

Sintering can be described into three separate stages: initial, intermediate, and final.[36] The initial stage of sintering has a rapid amount of neck growth until the neck radius is half the radius of the particle itself. This region occurs from the green body density of the material until around 0.65 relative density.[36] The intermediate stage describes the range of 0.65-0.9 relative densities. In this stage the pores are continuous but are starting to shrink and pinch of into individual pores. The final stage of sintering, taking place above 0.9 relative density, is where the induvial pores start to reduce volume and eventually disappear.[36,37]

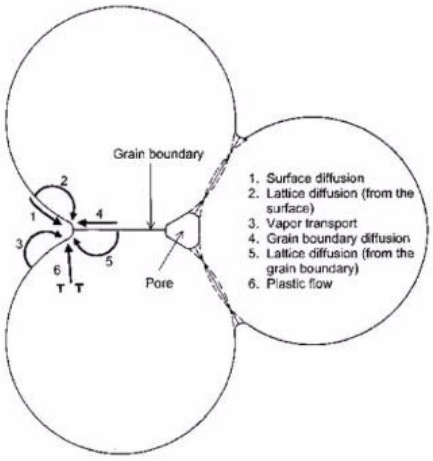

Figure 1.9: Illustration of the 6 different types of sintering mechanisms adapted from Rahman.[34]

For amorphous material, densifying through grain boundary and lattice diffusion would not apply, so a separate mechanism must be considered.[37] Viscous sintering is the mechanism that is applied to glass. This is where the material deforms, like plastic flow, to cause the necks to appear and grow.

Three common models are used to describe this densification behavior: Sherer, Frenkel, and Mackenzie & Shuttleworth models.[38-40] These models consider the viscosity characteristics of the glass, also including the surface energy of the material, as well as the average pore size. The Sherer and Frenkel models are good fits for initial and intermediate stages of sintering, where the Mackenzie & Shuttleworth (M&S) equation describes the final stage of sintering.[36]

A combination of the Frenkel and the M&S equations can be incorporated for a more complete look of the sintering curve for packed glass particle samples.[41] The Frenkel model is applied to all times before the sintering part reaches 0.8 the relative densities where the M&S covers the final stage of densification.

2. RESEARCH OBJECTIVE

The object of the research presented is to create hermetic glass-to-metal seals using additive manufacturing (AM) techniques. This is achieved through two separate routes: AM of the seal components and laser processing of the seals.

Additive manufacturing of the components utilizes SLM to produce 304L stainless steel shells and DLP to produce the glass preform. AM of both the metal and glass could bring the opportunity for different shell/preform geometries fitting a wider variety of applications.

Laser processing of the seal uses a Nd:YAG laser to heat a solid glass preform. The temperature the metal shell experiences in the laser processed seal is low compared to conventionally formed seals, reducing the compressive stresses from CTE mismatch. Additionally, the time to form a seal using the laser processing method is on the order of seconds, where furnace sealing methods generally dwell for a few minutes at the sealing temperature. This reduction of time will lessen the probability of a large interfacial layer forming, even with reactive metals. This would allow for a larger catalog of possible glass-metal combination.

PAPER

I. PRINTED GLASS PREFORMS FOR GLASS-TO-METAL SEALS

Aaron Read and Richard K. Brow

Department of Material Science & Engineering, Missouri University of Science & Technology, Straumanus-James Hall, 1400N. Bishop Ave, Rolla, MO 65409

ABSTRACT

Hermetic, single pin seals were made using metal shells produced by a selective laser melting (SLM) method and printed glass preforms by a digital light processing (DLP) method. The glass preforms were printed from a 2:1 weight ratio mixture of a silicate glass powder and a photosensitive acrylate resin. Organic removal and glass sintering schedules were determined from thermal analyses and video imaging techniques to create preforms for sealing. Densification curves for the sintered glass preforms were fit to viscous sintering models. Finally, a hermetic single pin seals were fabricated with the printed shells and preforms and Alloy-52 pins, using a conventional furnace-sealing process.

1. INTRODUCTION

1.1. GLASS-TO-METAL SEALS

Glass-to-metal (GtM) seals are used to create a hermetic barrier, often between metal pins and shells, for electronic applications.[1,2] Figure 1 shows a representative example of a single pin GtM seal.[3] Glasses are selected to be compatible with the metal components; for example, a sealing glass typically has a thermal expansion coefficient similar to that of the pin to reduce tensile stresses that might develop in the glass after sealing.[2,4,5] In a typical process, the seal is formed by heating the shell/glass/pin assembly to a high enough temperature to allow the glass to flow, then wet and bond to the metal components.[1,5] This process can limit the choices of materials that can be used to produce reliable GtM seals.

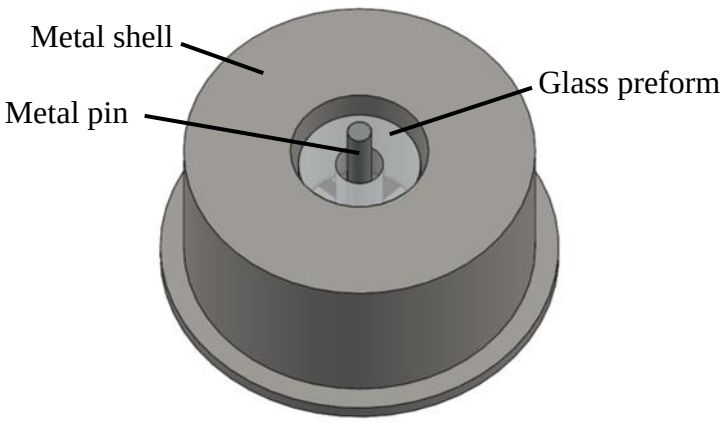

Figure 1: Schematic representation of a single pin glass-to-metal seal adapted from Brow.[3]

There are, in general, two types of glass preforms are used to fabricate GtM seals. For single pin seals, solid glass preforms that are cut from glass tubes to fit around the pin

and within the shell (Figure 1). During the sealing step, these preforms flow to fill the space between the pin and shell to a height determined by the glass volume and the fixturing used to hold the assembly. The other common glass preform uses powders mixed with organic binders that are pressed and then partially sintered into the final preform shape.[6,7] Seals are then fabricated with these preforms following similar procedures as those used for the solid glass preforms.

Additive manufacturing (AM) techniques are being used to produce components from a wide range of materials.[8] These AM components can geometries that are otherwise difficult to manufacture using typical subtractive methods. There are many different types of AM techniques.[9] The two techniques used in the present study are described here.

1.2. SELECTIVE LASER MELTING PROCESSING OF METAL SHELLS

Selective laser melting (SLM) is an AM method where a laser is used to melt a layer of powder to build, layer by layer, a monolithic part [10] Figure 2. shows a schematic drawing of the SLM process method.[11] The laser melts the powder layer, along with the top of the underlying substrate, to create a melt pool that then recrystallizes upon cooling. Each new layer is generally around 50 μm thick.[12] On cooling, a new powder layer is added, and the process repeats until the final monolithic piece is completed. In the present study, the SLM process was used to fabricate 304L stainless steel shells for GtM seals.

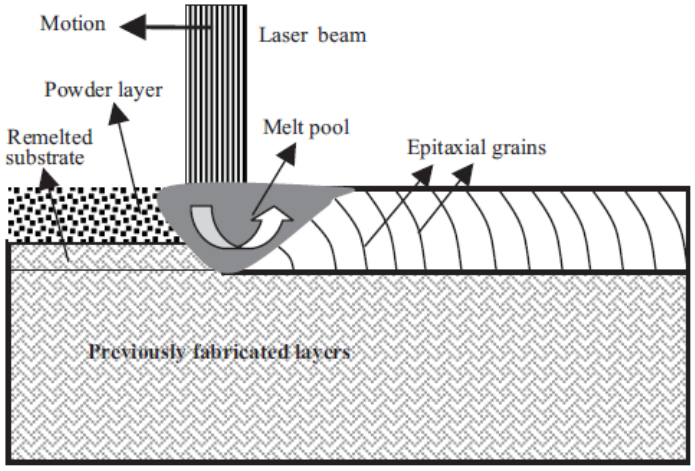

Figure 2: Schematic of the selective laser melting method shown by Das. S.[11]

1.3. ADDITIVE MANUFACTURING OF GLASS PREFORMS

There are a number of different methods to print glass parts from glass powders.[13-16] In many of these techniques, the glass powders are mixed with organic materials to create slurries that are then printed, layer-by-layer, to produce a monolith. That monolith then must be heated to remove the organics and to sinter the glass particles to a final density. In the present study, the digital light processing (DLP) method was used to print glass preforms for GtM seals. The organic used in this process is a resin that polymerizes when exposed to ultraviolet light. Once a layer of glass-loaded resin is cured on the build plate, a fresh layer of resin fills the gap between the cured part and the light source.[17] This repeats until the part is completed. Figure 3 is a schematic representation of the DLP process.[18]

In the present study, single-pin GtM seals were produced with metal shells printed by selective laser melting and glass preforms printed using the digital light processing technique. The ultimate goal of the project is to understand if additive manufacturing

techniques can produce GtM seals in geometries, or with material combinations, that are not suitable for more conventional sealing processes.

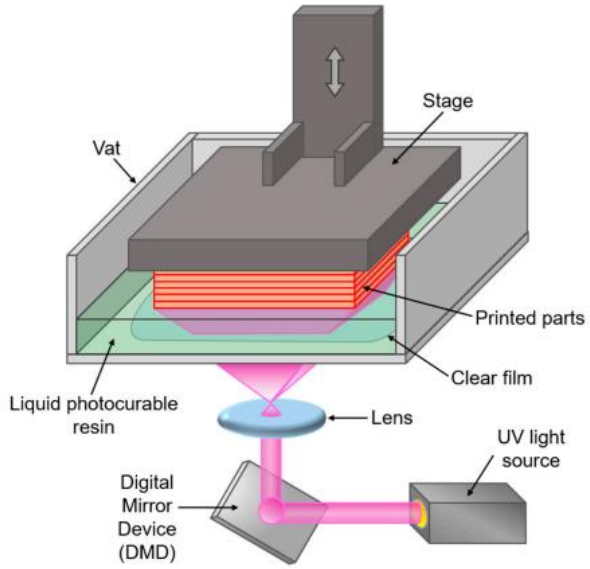

Figure 3: Schematic representation of the Digital Light Processing (DLP) printing shown by Bae.[18]

2. EXPERIMENTAL PROCEDURES

2.1. PRINTING METAL SHELLS

304L stainless steel powder (15-45 μm diameter, Carpenter Additive, Widnes, UK) was used to print shells with a 10 mm outer diameter, a 5.05 mm inner diameter, and a 5.5 mm height. The cylindrical shells were printed by a point-by-point SLM method using a Renishaw AM250 system (New Mills, Gloucestershire, UK). The shells were printed directly onto the build plate using the processing parameters summarized in Table 1. The shells were removed from the build plate using wire electronic discharge machining (EDM). An example of an as-printed shell is shown in Figure 4. The inner diameter was

machined with a 5.05 mm drill bit, and this was reported to reduce the surface roughness, Ra, from 7.2±1. µm to 3.5±1.3 µm.[3] The finished preforms were ultrasonically cleaned in ethanol for two minutes before being used to make GtM seals.

Table 1: Renishaw AM 250 laser parameters used to print 304L metal shells.

Laser Power (W)	Exposure Time (µs)	Hatch Spacing (µm)	Point Distance (µm)	Beam Width (µm)
200	75	85	60	50

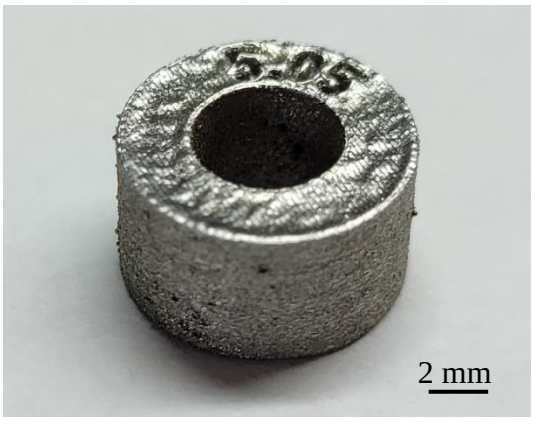

Figure 4: Image of an as-printed 304L stainless steel shell after removal from the SLM build plate by EDM.

2.2. GLASS CHARACTERIZATION

The sealing glass powder (Gl-1860, MoSci Co, Rolla, MO) is an alkali-barium-borosilicate glass designed to match the thermal expansion characteristics of the pin material, Alloy-52. The glass powder had an initial particle size (d_{50}) of 20.6 µm, reported by MoSci, and was then milled (8000M mixer/mill, SPEX SamplePrep,

Metuchen, NJ) for ten minutes using 5 mm spherical alumina media with a glass powder-to-media ratio of 1:2.75. After milling, the glass particle size (d_{50}) was determined (Microtrac S3500, York, Pa) to be 5.7 μm, as shown in Figure 5.

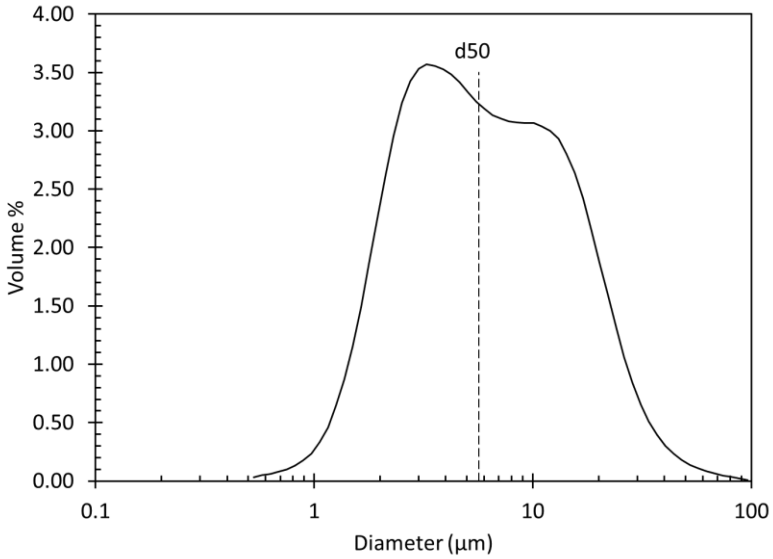

Figure 5: Particle size distribution of the Gl-1860 glass used for DLP printing.

Sixty-gram batches of as-received glass powders were added to a preheated (1000^{o}C), dense alumina crucible (AdValue Technology, Tucson, AZ), and then remelted at 1500°C for two hours. The resulting homogeneous, bubble-free melt was cast into a graphite mold (115 mm x 18 mm x 6 mm in dimensions) to produce a glass billet that was transferred to an annealing furnace set at 485°C and held for at least two hours, before cooling to room temperature.

5 mm diameter cylinders were core-drilled from an annealed billet, then cut to a height of 5 mm. These samples were used for thermal mechanical analysis (TMA) using a Perkin Elmer TMA 4000 (Waltham, MA). The cylinder was placed between two

platinum sheets, then heated in air at 10°C/min through the dilatometric softening point (T_{dil}) to collect the coefficient of thermal expansion (CTE, calculated over the range 200-400°C), the glass transition temperature and the dilatometric softening point. Other samples were held near T_{dil} (559°C) at 555°C for five minutes, then a uniaxial load (L) of 0.5 N was applied, the sample was heated at 2°C/min to 650°C, and the change of sample height (dh/dt, in m/s) was recorded in order to determine the glass viscosity, η (Pa*s) according to Equation 1.[19] Here V is the cylinder volume in m^3.

$$\eta = \frac{2\pi L h^5}{3V\frac{dh}{dt}(2\pi h^3 + V)} \quad (1)$$

Sample densities, ρ_s, were measured using the Archimedes method (ATSM C693-93), summarized by Equation 2,[20] with deionized water as the buoyancy fluid, ρ_m. The masses of the glass sample in air, w_a, and in the buoyancy fluid, w_b, were used for the calculation.

$$\rho_S = \frac{w_a \rho_m}{w_a - w_b} \quad (2)$$

2.3. GLASS-RESIN FORMATION AND CHARACTERIZATION

Milled glass powder was mixed with an acrylate base resin (Genesis High Load Development Resin Base, Tethon 3D, Omaha NE) in a 2:1 glass:resin weight ratio. The specific gravity of the resin, as reported by Tethon, was 1.17 g/cm^3. The powder was slowly added to the resin while it was being stirred with a paint mixer attached to drill, and this continued until the final glass:resin mixture was visibly homogeneous.

The glass-resin mixture was characterized in both air and nitrogen atmospheres by simultaneous thermo-gravimetric analysis (TGA) and differential scanning calorimetry

(DSC) using a Netzsch STA 449 (Selb, Germany), and a ramp rate of 10^{o}C/min up to 700^{o}C.

To avoid settling of glass particles, the glass-resin mixture was immediately printed after mixing. The Bison 1000 (Tethon 3D, Omaha NE) printer was used to produce the green preforms using the parameters given in Table 2 shows that were used to print each preform. The first six layers were printed with slightly longer UV-curing times and longer hold times than the subsequent layers. Each layer was about 50 microns thick. Twenty individual preforms were printed in each run, taking about two hours.

Table 2: DLP printer settings to produce glass:resin preforms. The first times indicated were used to print the first six layers of the preform and the second times were used to print all subsequent layers.

Printing Parameter	
Curing times (seconds)	80, 65
Hold times (seconds)	60, 55

Preforms were printed with dimensions that were 23% larger than the final desired dimensions of the densified parts. Table 3 summarizes the target and printed dimensions of the preform cylinders.

After printing, the preforms were removed from the build plate using a metal blade and the excess resin was removed with a paper towel. The center holes were cleaned with a 0.8 mm diameter metal rod. The preforms were rinsed in isopropyl alcohol for two minutes then dried in air overnight.

Table 3: Programed (target) and actual (measured) dimensions of the as-printed glass:resin preforms. Sample population size of 20 was used.

Dimension	Target size (mm)	Measured size (mm)
Outer diameter	6.15	6.23±0.62
Inner diameter	1.66	1.79±0.05
Height	4.92	4.86±0.05

2.4. BURNOUT AND SINTERING OF PRINTED GLASS PREFORMS

Printed preforms were slowly heated in air to remove (burnout) residual organic materials and to partially sinter the glass particles. The details of these treatments are described below in the results and discussion section. The effects of temperature on the dimensions of the preforms were characterized using a video imaging technique. Preforms were positioned on a platinum sheet in a window furnace (Paragon Industries, Mesquite TX) that was ramped to 1000^{o}C at a rate of 5^{o}C/min, while a camera (Basler Inc., Exton, PA) recorded an image every 15-60 seconds. Figure 6 shows the camera/furnace set-up. Cross-sectional areas of the images were analyzed using the image processing software, ImageJ (version 1.53e, National institutes of Health, USA).

Images were also collected every 30-60 seconds for two hours during a series of isothermal treatments at 615^{o}C, 630^{o}C, and 645^{o}C. In these experiments, preform densities were calculated from the cross-sectional areas, and the final mass of the sintered preforms. The cross-sectional area was converted to a volume for the preform, assuming the preform was a cylinder and the inner diameter changes in dimension at the same rate as the outer diameter. The final mass of the preform after sintering was divided by the

calculated volume to get a density and compared to the density measured by the Archimedes method.

Figure 6: Image of a camera setup for the measuring the cross-section of sintering preforms.

2.5. SEALING CONDITIONS AND HERMETICITY TESTING

The printed metal shells, printed and sintered glass preforms, and Alloy-52 pins (National Electric Wire Co., Toms River NJ) were assembled in the single-pin configuration shown in Figure 1. The dimensions of the seal parts are shown in Table 4. The glass preforms were supported by a graphite spacer to prevent the glass from flowing out of the shell. The seal assembly was loaded into a tube furnace (Thermal Technology LLC, Minden, NV) under a flowing Ar atmosphere. The seals were heated using the schedule shown in Table 5.

Table 4: Dimensions of the 304L shells, desired printed glass preforms, and alloy 52 pins used to create single pin seals.

Part	Outer Diameter (mm)	Inner diameter (mm)	Height (mm)
Shell	10.0	5.05	6.5
Glass preform	5.0	1.5	4.0
Alloy 52 pin	1.0	---	10

Table 5: Firing schedule for making single pin GtM seals.

Ramp Rate (^{o}C/min)	Temperature (^{o}C)	Hold (min)
20	980	12
30	460	-
5	100	-

Once cooled, the seals were visually inspected and then tested for hermeticity using a Varian 979 helium leak detector. A custom fixture, shown in Figure A.1 in the appendix, was used to measure the leak rates through the seals, and these values were compared to that measured through a solid Al plug positioned in the same fixture. Leak rate values within an order of magnitude of 1.2 of the Al plug were considered hermetic. Further explanation in the Appendix.

3. RESULTS AND DISCUSSION

3.1. GLASS PROPERTIES

21 bubble-free samples of annealed bulk glass pieces were analyzed for their density using ASTM C693-93.[20] The density of the samples were found to be 2.61±0.02 g/cm^3.

Representative TMA data for the Gl-1860 glass are shown in Figure 7, which indicate that the glass transition temperature (T_g) is 460±4^{o}C, the thermal expansion (CTE) between 200-400^{o}C is 108±9x10^{-7}/^{o}C, and the dilatometric softening point is 559±3^{o}C. These characteristic thermal properties are based a total of 3 TMA data sets collected from annealed samples.

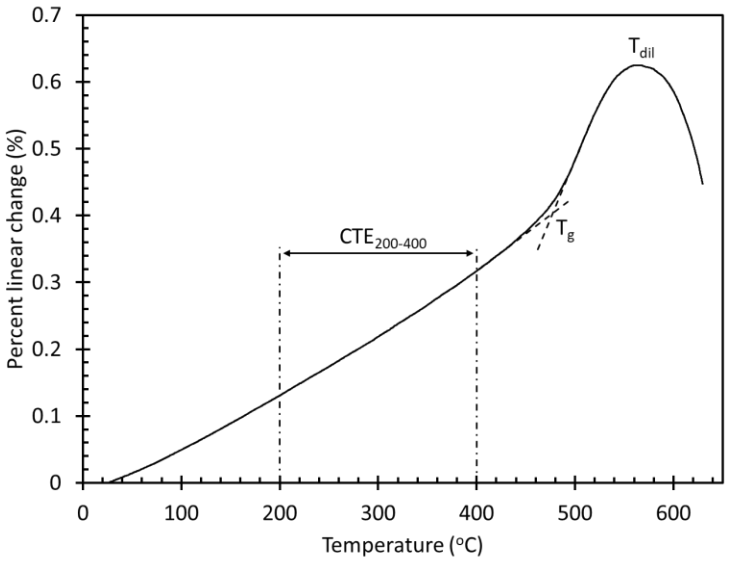

Figure 7: TMA data for the Gl-1860, showing the range of temperatures used to calculate CTE and the characteristic temperatures.

Figure 8 shows the viscosity data measured for Gl-1860 glass. This viscosity data, η (Pa*s), along with the glass transition temperature measured by TMA (Figure 3.1), were fit to the MYEGA viscosity model, Equation 3.[21] Here $log_{10}\eta_{\infty}$ is a value of -3.5 log (Pa*s) and the fragility of the glass, m, was fit to the data. Table 6 shows the MYEGA viscosities calculated for Gl-1860 for the isothermal temperatures used for sintering.

$$log_{10}\eta(T) = log_{10}\eta_{\infty} + (12 - log_{10}\eta_{\infty})\left(\frac{T_g}{T}\right) exp\left[\left(\frac{m}{12-log_{10}\eta_{\infty}} - 1\right)\left(\frac{T_g}{T} - 1\right)\right] \quad (3)$$

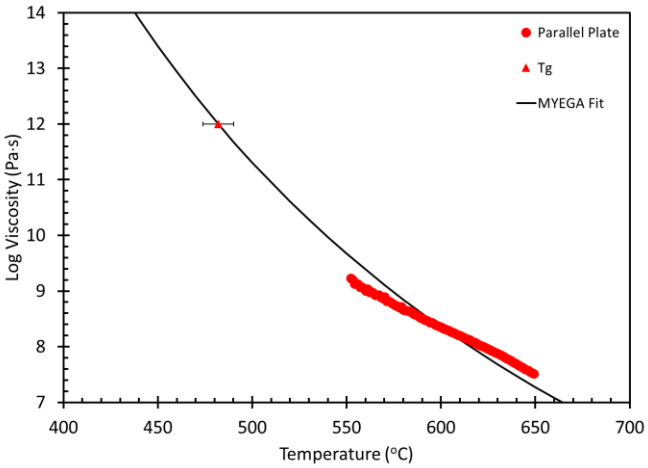

Figure 8: Viscosity of Gl-1860 as a function of temperature measured with TMA. MYEGA fit applied to the TMA data and the measure glass transition temperature (T_g).

Table 6: Viscosity values at three temperatures: 615°C, 630°C and 645°C from the MYEGA fit on the TMA data.

Temperature (°C)	MYEGA η log(Pa*s)
615	8.01
630	7.69
645	7.38

3.2. TGA/DSC OF RESIN

Figure 9 shows the TGA data collected from the glass-resin mixture heated in both nitrogen (dashed orange line) and in air (solid blue line). The initial mass loss occurs at a lower temperature in nitrogen but the total mass loss at 700°C was greater (33.3%) in air than in nitrogen (31.9%). The glass:resin mass ratio in these samples was 2:1, indicating that some residual material likely remained in the sample heated in nitrogen.

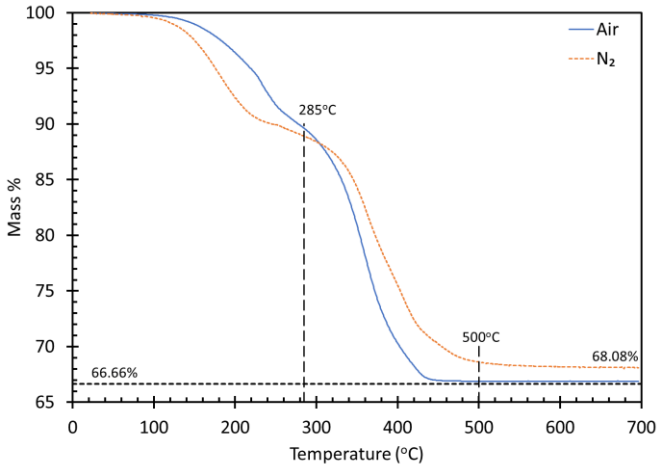

Figure 9: TGA data for the glass-resin mixture (by mass, 2:1) collected in air (blue solid line) and in N_2 (orange dashed line).

Figure 10 shows the DSC data that were simultaneously collected with the TGA data on the glass:resin mixture in air and in nitrogen. For the data collected in air (solid blue line), there are several exothermic features, with peaks near 260, 370 and 420°C. For the sample run in nitrogen (dashed orange), the initial peak is at a lower temperature (230°C), followed by broad features centered near 370°C and 600 °C. These data trends are similar to thermo-analytical data reported in the literature.[22] The first exothermic peak, 230-260°C, is most likely due to acrylate polymerization expected to occur both in

air and N_2 atmospheres.[22] The sharp exothermic peaks near 370°C and 420°C in the DSC data collected in air are likely due to the oxidation and thermal decomposition of organics in the resin;[23,24] these exotherms are associated with the large mass loss between 300-450°C noted in the corresponding TGA data in Figure 9 In the nitrogen atmosphere, oxidation is suppressed and the thermal decomposition leads to the much more gradual, and ultimately incomplete weight loss noted in the TGA data.[25]

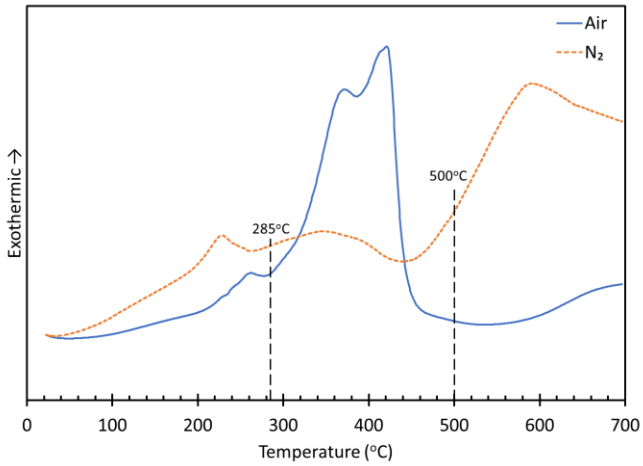

Figure 10: DSC data for the glass-resin mixture collected in air (blue solid line) and in N_2 (orange dashed line).

3.3. BURNOUT SCHEDULE

The thermal analysis data shown above were used to design the resin burnout schedule for the printed preforms. The TGA and DSC data indicate two temperature ranges where significant mass loss and exothermic reactions occur: from room temperature to about 300°C, then between 300°C and about 500°C. A series of screening experiments were done using different ramp rates and hold times to optimize the overall burnout process; those parameters are summarized in Table 7. The two hold temperatures

were fixed at 285°C and 500°C, corresponding to the temperatures of the onset and the end of the second large mass loss and bracketing the most significant exothermic processes in air. The initial slow ramp rate to 285°C and subsequent hold were intended to allow the controlled release of organics that produce the initial mass losses detected by TGA.[26] The slow ramp rate to 500°C and subsequent hold were intended to allow the controlled release of remaining organic materials associated with the higher temperature range of exothermic mass loss.[27]

Table 7: The four parameters considered to reduce defects in the organic burnout step of the preform sintering process.

Step Process	Range of values
Ramp rate to 285°C	0.25°C/min to 5°C/min
Hold time at 285°C	30 min to 5hrs
Ramp rate to 500°C	1°C/min to 5°C/min
Hold time at 500°C	30 min to 5hrs

Burnout samples were evaluated by their color, mechanical stability (flaking and cracking), and final weight change. Figure 11a shows a preform that had an initial ramp rate of 5°C/min; it was split and had some charring. Cracking is a consequence of the expansion of the organic phase and the charring results from the incomplete burnout of the organics.[28] Figure 11b shows a preform that had an initial ramp rate of 0.25°C/min. This sample shows some surface flaking, but better structural integrity than the faster initial ramp rate. The slower ramp rate is similar to reported binder burnout schedules for ceramic parts.[26] From these screening experiments, the following burnout schedule was

adopted for the preforms used in the sintering and sealing experiments described in the following section.

- 0.25°C/min to 285°C and held for 2 hours
- 1°C/min to 500°C and held for 5 hours.

This schedule produced preforms that were light grey-to-white in color and that lost, on average, 31.9±1.1 wt% (n=6).

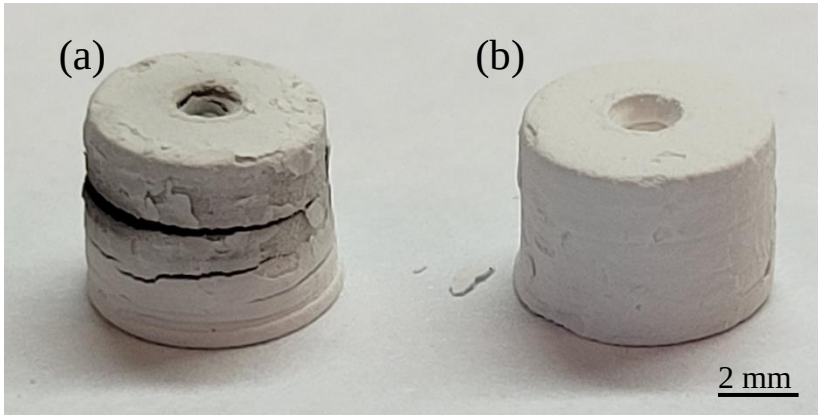

Figure 11: Printed preforms after (a) a fast ramp rate burnout and (b) a slow ramp rate burnout.

3.4. DENSIFICATION AND PREFORM SINTERING SCHEDULE

Figure 12 shows examples of the images collected from a preform that had undergone a burnout treatment and then was heated in air at 5°C/min to 1100°C. The image collected at 500°C (Fig. 12a) shows the sample before densification starts, and the image collected at 700°C (Fig. 12b) shows a densified sample. At 800°C (Fig. 12c), the sample was bloated, and then collapses at 1050°C (Fig. 12d). Figure 13 shows how the normalized cross-sectional area of the sample from Figure 12 varied as a function of temperature. Here, the onset of densification appears near 600°C and continues at least up

to 700°C. The onset of densification occurs above the dilatometric softening temperature of Gl-1860 (Figure 7). The sample deformed some up to about 770°C when significant bloating commenced. The sample remained bloated up to about 950°C, where it began collapsing, eventually wetting and spreading on the platinum substrate.

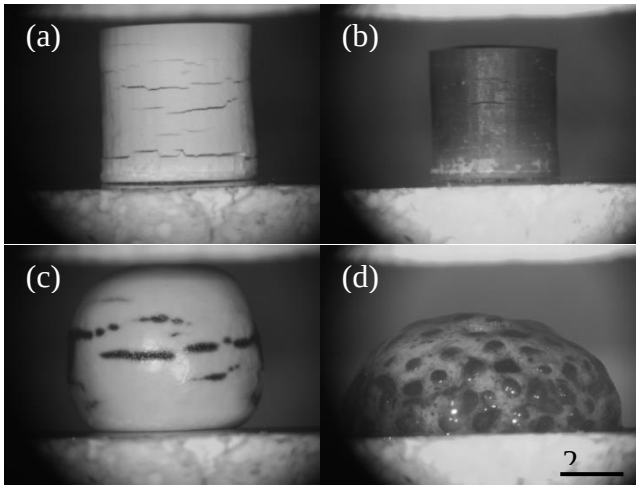

Figure 12: Images of a preform heated from room temperature at 5°C/min, captured at (a) 500°C, (b) after densifying at 700°C, (c) after bloating at 880°C, and (d) and after collapsing at 1050°C (d).

A series of isothermal experiments were done between 615°C to 645°C to characterize preform densification. Preforms were heated at 5 °C/min to the target temperature and then images were collected under isothermal conditions for two hours as the samples densified. Figure 14 shows how the normalized cross-sectional areas of a preform changed as a function of time at 615°C, 630°C, and 645°C. In each case, the samples decreased in size, with the densification rates increasing with temperature, before reaching a plateau.

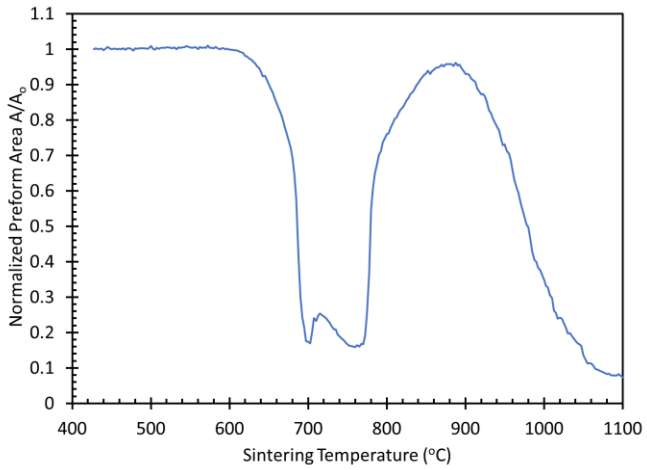

Figure 13: Normalized cross-sectional areas of a preform heated from room temperature to 1100°C at 5°C/min ramp. The onsets of densification and sample bloating occur near 600°C and 770°C, respectively.

At the conclusion of the isothermal hold experiments, the sintered preforms were inspected and then their densities were determined. Figure 15 shows an example of a sintered preform after 2 hours at 630°C. The sintered preforms had a light grey/brown color after sintering and were opaque. This indicated that some of the organics from the resin were not completely burned out or that there was some char residue coating the glass particles in the preform.[24]

The dimensional changes shown in Figure 14 were used with the respective sample masses to calculate the time dependence of sample density for the isothermal experiments. The height and diameter from each cross-section were used to calculate the geometric volume of the preform, assuming the outer and inner diameters reduced size at the same rate. Figure 16 shows how the relative density changed with time for preforms isothermally heated at 615°C, 630°C, and 645°C. In general, each sintered sample reached about 0.97 theoretical density, 2.52±0.03 g/cm^3, after two hours at 615°C, 630°C, and 645°C. Table 8 shows that the time required to reach 0.97 relative density decreases from

about 96 minutes to about 22 minutes when the isothermal sintering time was increased from 615 to 645ºC. Full density was not achieved because of bubbles trapped in the preform. These bubbles contribute to the visible opaqueness of the samples.

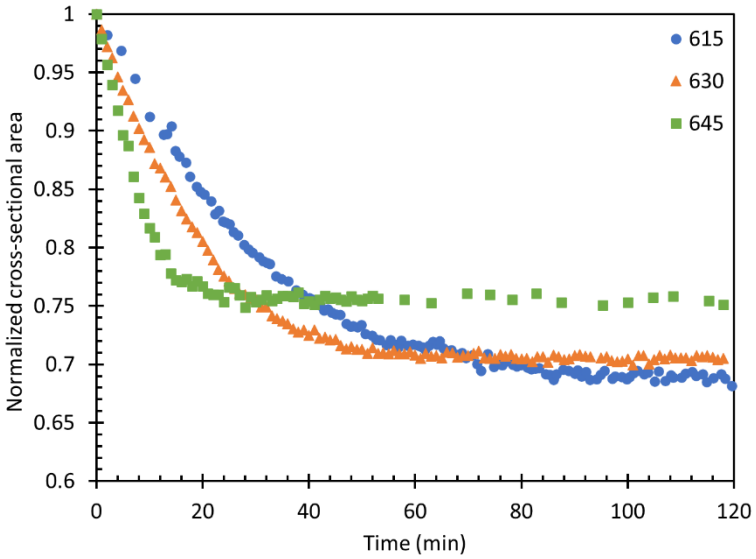

Figure 14: Cross-sectional area, normalized to the dimensions of the preform after organic burnout, evaluated over time for preforms sintered at 615, 630 and 645ºC.

Figure 15: A Gl-1860 preform after sintering for 2 hours at 630ºC.

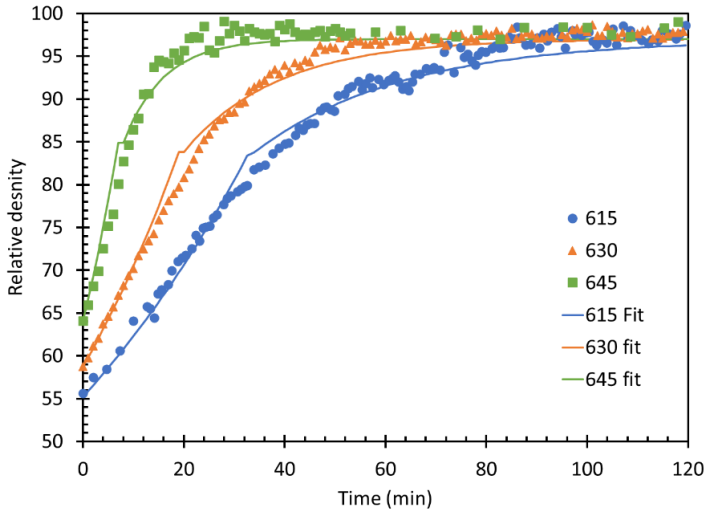

Figure 16: Densification curves for Gl-1860 preforms from the isothermal sintering experiments. The lines are fits to sintering models described in the text.

Table 8: Time needed for the printed preforms to reach 0.97 relative density and viscosity of the glass-preforms at various isothermal hold determined by the viscous sintering model, and TMA analysis.

Sintering Temperature (°C)	Time (min)	Viscous sintering Log(Pa*s)	TMA η log(Pa*s)
615	96	8.82	8.12
630	62	8.65	7.89
645	22	8.31	7.59

The faster sintering kinetics at higher temperatures can be related a decrease in glass viscosity. Viscous flow controls glass densification.[28] Models for viscous flow uses a reduction in surface energy as a driving force for densification and the glass viscosity as controlling the densification rate. A hybrid model that uses the Frenkel model to describe the initial stages of sintering, up to 0.8 relative density, and the Mackenzie and

Shuttleworth (M&S) model for the final stages of sintering, has been developed for glass particles and is described by Equation 4: [29-31]

$$\rho(t) = \frac{\rho_o}{\rho_g\left(1-\frac{3\gamma t}{8\eta(T)r}\right)^3}\theta(t_{0.8}-t) + \left(1-\exp\left(\frac{-3\gamma t}{2a_o(r)\eta(T)} + \ln\left(1-\frac{\rho_o}{\rho_g}\right)\right)\right)\theta(t-t_{0.8}) \quad (4)$$

Here, ρ_o and ρ_g are the initial density of the preform and the density of the bulk glass, respectively; γ is the glass-vapor surface energy and a value of 0.327 J/m^2 was used here;[31] r is the initial radius of the glass powder, and the d_{50} value of the milled powder (2.83 µm) was used. The θ terms are step functions where $\theta(t_{0.8}\text{-}t)$, used in the Frenkel model, is 1 for times until 0.8 relative density is reached, and then the value changes to 0. The values are reversed for $\theta(t\text{-}t_{0.8})$ used with the M&S model. The value of $a_o(r)$ was chosen to minimize the difference between the Frenkel and M&S models at $t=t_{0.8}$. $\eta(T)$ is the temperature dependence of viscosity, Pa*s was varied to improve the fit of the model to the data trends.

The values for viscosity from the viscous sintering model are about a 0.75 an order on magnitude higher than the measured TMA viscosities, Table 8. This difference could be due to the TMA parallel plate measurements being less accurate at lower temperatures or the viscous sintering model used only accounts for the mean particles size.[19,32] The viscous sintering model used by Prado et. al. accounted for the particle distribution due to smaller particles sintering faster than the larger glass particles.[32]

The chosen burnout schedule implemented reduced the number of defects seen from slow ramp rates and long hold times at the hold temperature, 285°C and 500°C, with a near complete removal of organics. A sintering schedule of 5°C/min to 630°C, held for two hours saw preforms, example in Figure 16, reaching 0.97 relative density. This

schedule was used for creating the seals. Dimensional shrinkage of the as-printed size to final densities of the preforms that underwent the recommended heat treatments, Table 9.

Table 9: Percent shrinkage of the as-printed preform dimensions after sintering.

Dimension	Sintered Shrinkage (%)
Outer diameter	21.4±2.1
Inner diameter	20.7±2.3
Height	23.2±1.9

3.5. HERMETIC SEAL FABRICATION

Three single-pin seals were produced with a printed shell, a sintered glass preform, and an Alloy-52 pin, Figure 17. Three of the four samples were hermetic, with an average He leak rate of $1.2\pm0.4 \times 10^{-7}$ atm-cc/sec, compared to a leak rate of 1.2×10^{-8} atm-cc/sec for the Al plug. The preform had a good wetting behavior with metal, indicating the bond had a good adherence.[32]

The glass preform in Figure 17 is clear but has many bubbles, shown clearly in Figure 18. During sealing the remaining organics and char from the sintered preform evolved off. The bubbles in the glass, 50-100 μm, were formed by the organic removal. These bubbles could cause additional stress from rapid gas expansion if the seal is thermally cycled. A longer hold time at the sealing temperature, 980°C, would allow for a bubble free, defense perform.

Figure 17: Hermetic ingle pin seal produced with a DLP printed glass preforms, an SLM printed 304L shell, and an Alloy-52 pin.

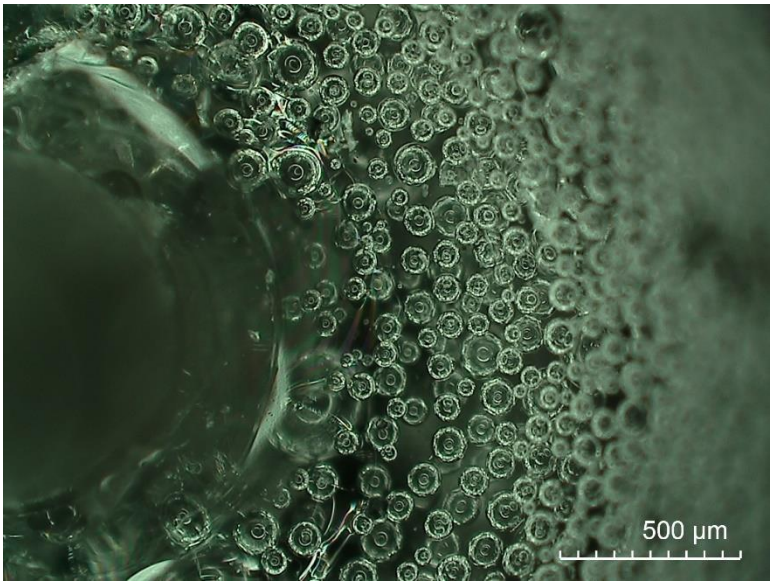

Figure 18: Optical image of the top surface of a printed preform seal showing the bubbles trapped in the glass.

4. SUMMARY

Glass preforms were fabricated using a digital light processing technique.

TGA/DSC data provided information used to design the organic burnout schedule. Image

analyses provided quantitative dimensional information on green preforms heated to 1100ºC and this was used to develop the sintering cycles needed to produce the final preforms. A viscous sintering model was used to analyze isothermal densification rates and related to measured glass viscosities. Finally, single-pin seals were fabricated using the DLP printed and sintered glass preforms, 304L stainless steel shells, and Alloy-52 pins. The seals had bubbles, but showed good wetting to the shells and pins and were hermetic, as determined by helium leak tests.

REFERENCES

1. Donlad I. *Glass-to-metal seals*. Soc. Glass Technol. (2009)
2. Rulon, R. *Introduction to Glass Science*. Plenum Press. p. 661–704. (1972)
3. Brow R., Bai J., Lough C., Wang W. *Final report to Honeywell FM&T.* (2020)
4. Partidge G. Glass-to-metal seals. Soc. Glass Technol. (1949)
5. Hull A., Burger E. *Physics*. 5(12): 383. (2004)
6. Gong K., et. al. *Mat. Res. Express*. 10(2): 5201 (2023)
7. Donald, I. W. *J. Mat. Sci*. 28(11): 2841. (1993)
8. Singh S., Ramakrishna S., Singh R. *J. Manu. Proc*. 25:185. (2017)
9. Wong K., Hernndez A. *ISRN Mech. Eng.* 2012(208760): 10. (2012)
10. Kruth JP., et. al. *J. Mat. Proc. Tech*. 149(1):616. (2004)
11. Das, S. *Advanced Engineering Materials*. 5(10): 701. (2003)
12. Sufiiarov, V., et al. *Procedia Engineering*. 174(Jan): 126. (2017)
13. Zhang D., Liu X., Qiu J. *Front Optoelectron*. 14(3):263. (2021)

14. Cai P, Guo L, Wang H, et al. *Ceramics International*. 46(10, Part B):16833. (2020)

15. Fu Q, Saiz E, Tomsia AP. *Acta Biomaterialia*. 7(10):3547. (2011)

16. Datsiou KC, Saleh E, Spirrett F, et.al. *J. Am. Ceram. Soc*. 102(8):4410. (2019)

17. Baumgartner S., Gmeiner R., Schönherr JA., Stampfl J. *Mate. Sci. Eng.: C*. 116:111180. (2020)

18. Bae S., Kim B. *Appl. Sci.* 11:6835 (2021)

19. Fontana E. *Ceram. Bull.* 49(6):594. (1970)

20. ASTM C693-93, "Standard Test Method for Density of Glass by Buoyancy", ASTM International, West Conshohocken, PA. (2019)

21. Mauro J., Yue Y., Ellison A., Gupta P., Allan D. *PNAS*. 106(47):19780. (2009)

22. Hafsa MN, Ibrahim M, Sharif S. *IOP Conf Ser: Mater Sci Eng*. 50(1):012059. (2013)

23. R. Gilissen and A. Smolders. *High Tech. Ceramics*. p567. (1987)

24. Cima M., Levis J. *Ceram. Trans.* 1:567. (1988)

25. Prabhakaran K, Pavithran C. *J. Euro. Ceram. Soc*. 20(8):1115. (2000)

26. Zhang J., Edirisinghe M., Evan J. *Mater. Lett.* 7:15 (1988)

27. Strangle G., RheeD., Aksay I. *Proceedings of ANTEC89, Society of Plastics*. :1066 (1989)

28. Rahaman M. Sintering of Ceramics. CRC press. (2008)

29. Frenkel J. *Phys*. 9[S]:385. (1945)

30. Mackenzie J., Shuttleworth R. *Proc. Phys. Soc.* 62:833. (1949)

31. Prado M, Zanotto E, Müller R. *J. of Non-Crystalline Solids*. 279(2):169. (2001)

32. Durpé A. *Theorie Mechanique de la Chaleur,* Gautheir-Villars, Paric (1869)

II. LASER ASSISTED MANUFACTURING OF GLASS-TO-METAL SEALS

Aaron Read and Richard K. Brow

Department of Material Science & Engineering, Missouri University of Science & Technology, Straumanus-James Hall, 1400N. Bishop Ave, Rolla, MO 65409

ABSTRACT

Glass-to-metal seals form hermetic barriers between components in a device and are often used for electronic applications. Conventional furnace manufacturing of seals restricts the choice of materials and design of the seal to ensure desired reliability. A laser assisted manufacturing (LAM) method was investigated as an alternative approach to producing glass-to-metal seals. A commercial sealing glass was modified by the addition of oxides, Fe_2O_3 or CuO, to increase absorption at the wavelength of the Nd:YAG laser used for the LAM process. Processing conditions that produced hermetic seals, determined by helium leak testing, were determined. The glass-metal interfaces of seals made by both the LAM process and by conventional furnace processing were characterized by analytical electron microscopy, which revealed the presence of reduced metal droplets at the LAM interfaces, and an oxide layer at the interfaces of the furnace-manufactured seals.

1. INTRODUCTION

1.1. GLASS-TO-METAL SEALS

Glass-to-metal (GtM) seals are hermetic components composed of three primary components: a metal shell, glass preform, and metal pin.[1,2] An example of a single pin seal is shown in Figure 1.[3] Glass is used as the hermetic barrier because of its desirable electrical properties, chemical stability, and thermal and mechanical properties, including thermal expansion coefficient, that are compatible with the metal components.[2,4] Conventional GtM seals are made be heating an assembly to a high enough temperature to allow the glass to flow, wet, and then bond to the respective metal interfaces.[1]

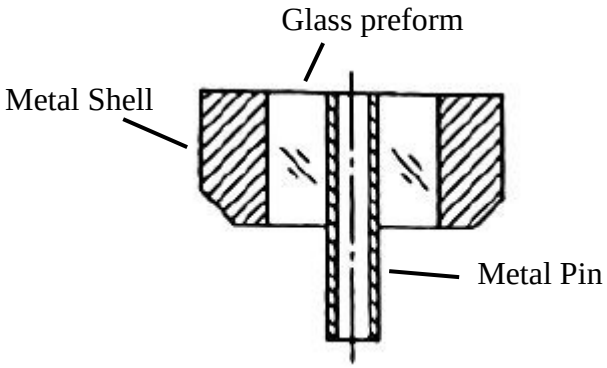

Figure 1: Schematic of simple single pin seal with e metal surrounded by the glass preform, encapsulated with metal shell adapted by Tomsia.[3]

1.2. CHEMICAL BONDING AT GLASS-METAL INTERFACES

A good quality seal will have a chemical bond between the glass and the metal and will avoid the formation of tensile stresses that might arise from mismatches in the thermal contraction characteristics of the materials when they are cooled after sealing.[4,5] The chemical bond can form a interfacial layer by redox reactions between the metallic

components and oxides in the glass, as well as reactions with the atmosphere when the seals are produced.[6] Alkali oxides or an in the glass composition or transition metal oxides that are purposefully doped into the glass can be reduced by reactions with metals.[6,7] Under some conditions, the reduced alkalis can be volatilized from the glass-metal interface.[8] Easily reduced oxides, like CuO, can be added to sealing glasses to create an oxide bond at the metal interface of a seal.[1] The oxide within donates its oxygen to the metal and the interfacial metal oxide until it reaches its saturation for the glass, then diffuses into the bulk of the glass .[6]

Reactive metals readily form thick interfacial oxides when sealed to oxide glass.[9] Thick interfacial layers could have a deleterious effect on seal reliability either by forming a leak path that limits hermeticity or by generating stresses because of mismatched thermal properties.[10] Ideally this reaction layer will be a mono-atomic thick layer.[6]

1.3. LASER MANUFACTURING OF GLASS-TO-METAL SEALS

To circumvent some of the issues that rise from a conventional furnace sealing process, laser assisted manufacturing (LAM) techniques could be used. An incident laser would heat the glass to its sealing temperature through a volumetric heating process, which depends on the absorptivity, α, of the glass at the laser wavelength, Equation 1.[11]

$$q'' = \alpha \frac{2P}{\pi r_o^2} \exp\left[-2\left(\frac{R}{r_o}\right)^2\right] \quad (1)$$

Here, q″ is the heat flux on the surface of the glass, P is the power of the laser, and r_o and R are the laser waist diameter and the distance from the beam center,

respectively. Heating during the LAM process is on a shorter time scale compared to conventional furnace sealing processes. This reduction in time could reduce the growth of a thick interfacial layer forming, potentially expanding the combinations of metals and glasses used to fabricate hermetic seals.

1.4. OPTICAL PROPERTIES OF THE GLASS TO MATCH LASER PROCESSING CONDITIONS

Metal oxide dopants can be added to a glass to increase its absorbance at the laser wavelength. In the present study, a Nd:YAG laser is used for LAM processing, and it operates at 1064 nm. Ferrous ions (Fe^{2+}) in silicate glasses absorb in the near-infrared (near-IR).[12] Ferric ions (Fe^{3+}) absorb in the near-ultraviolet.[13] To reduce ferric ions to ferrous ions, a reducing agent like SnO can be added to the glass to force the following redox reaction to the right:[14]

$$2Fe^{3+} + Sn^{2+} \rightarrow 2Fe^{2+} + Sn^{4+} \quad (2)$$

CuO can also be added to a glass to increase the near-IR absorption. The peak absorption for Cu^{2+} ions in silicate glasses is about 780 nm, but these peaks are broad and their tails extend into the near IR, Figure 2.[15]

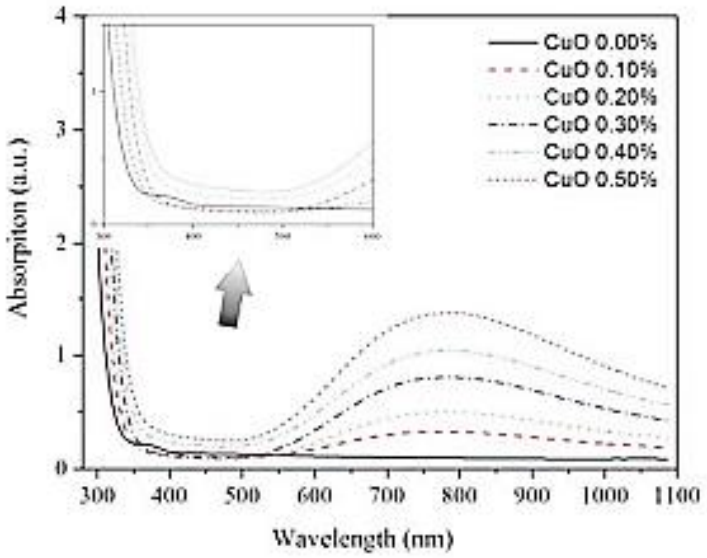

Figure 2: Absorbance spectra of CuO doped soda-lime-silicate shown by Wongsing and Kaewkhao.[15]

2. EXPERIMENTAL PROCESSING

2.1. PREPARING GLASS PREFORMS AND OTHER GLASS SAMPLES

Powders from a commercial alkali barium borosilicate sealing glass (Gl-1860, Mo-Sci Corp., Rolla, MO) were batched with various amounts of CuO (A.C.S reagent >99% purity, Aldrich Chemical, St. Louis, MO) or Fe_2O_3 (Grade 1 purity, Johnson Matthey Chemical Products, Royston, UK). The iron-doped glasses were co-doped with SnO (99.5% purity, Alfa Aesar, Haverhill, MA) at a 1:1 molar oxide ratio of Fe_2O_3:SnO to promote the reduction of ferric ions to ferrous ions (Equation 2). Table 1 shows the batch compositions of the glasses prepared in this study.

Table 1: Batch compositions, in wt%, of the glasses used to form seals to absorb the Nd:YAG laser wavelength, 1064nm.

Glass Name	wt% Gl-1860	wt% CuO	wt% Fe2O3	wt% SnO
1.5 wt% Fe_2O_3	97.23	---	1.50	1.27
1.0 wt% Fe_2O_3	98.49	---	1.00	0.51
0.5 wt% Fe_2O_3	99.25	---	0.50	0.25
1.5 wt% CuO	98.50	1.50	---	---
1.0 wt% CuO	99.00	1.00	---	---
0.5 wt% CuO	99.50	0.50	---	---

Sixty-gram batches, including dopants, were added to a preheated (1000^{o}C), dense alumina crucible (AdValue Technology, Tucson, AZ), and then were melted in air at 1500°C for two hours. The resulting homogeneous, bubble-free melts were cast in a graphite mold (115 mm x 18 mm x 6 mm in dimensions) to produce glass billets that were transferred to an annealing furnace at 485°C and held for at least two hours, before cooling to room temperature.

After annealing, the glass billets were core-drilled to form hollow cylindrical preforms with outer diameters of 5.0 mm, inner diameters of 1.5 mm, and heights in the range 3.8-4.2 mm, or solid cylinders with the same outer diameters and heights. The glass preforms were polished on top and bottom surface using silicon carbide polishing pads to a 1200 grit finish.

Wafers about 1 mm thick were sliced from the annealed billets and were polished on both sides to a 1 μm diamond slurry finish (Buehler, Lake Bluff, Il). Optical absorbance measurements were made on these polished wafers in the range of

wavelengths from 300 to 1100 nm using a Genesys 10 UV spectrometer (Thermo Scientific, Waltham MA).

Thermal mechanical analyses (TMA) of solid preforms, 5mm tall, were done using a Perkin Elmer TMA 4000 (Waltham, MA). A cylinder was placed between two platinum sheets, then heated in air at 10°C/min through the dilatometric softening point (T_{dil}) to collect the coefficient of thermal expansion (CTE, calculated over the range 200-400°C), the glass transition temperature (T_g), and (T_{dil}). Three samples of the undoped Gl-1860, 1.5wt% Fe_2O_3, and 1.5wt% CuO were tested.

The densities of the bubble-free, optical absorbance wafer samples were measured using the Archimedes method (ATSM C693-93)[16] with deionized water as the buoyancy fluid. The specific gravity of water at room temperature, ρ_m, and the masses of the glass samples in air, w_a, and in the buoyancy fluid, w_b, were used to calculate the glass density, according to:

$$\rho_s = \frac{w_a \rho_m}{w_a - w_b} \tag{3}$$

2.2. FABRICATING SEALS USING THE LASER ASSISTED MANUFACTURING METHOD

Single-pin GtM seals were produced by the LAM sealing method using 304L stainless steel shells, printed by the selective laser melting (SLM) method, doped sealing glass preforms, and Alloy-52 pins (National Electric Wire Co., Toms River NJ). The SLM shells were printed with 304L stainless steel powder (15-45 µm, Carpenter Additive, Widnes, UK) in a Renishaw AM 250 (New Mills, Gloucestershire, UK) using a 200 W Nd:YAG laser with a point-by-point methodology, spacing the points 60 µm and

holding for 100 µs. The dimensions of the individual components are summarized in Table 2.

Table 2: Dimensions of the 304L shells, glass preforms, and alloy 52 pins used to create single pin seals.

Part	Outer diameter (mm)	Inner diameter (mm)	Height (mm)
Shell	10.0	5.05	6.5
Glass preform	5.0	1.5	3.8-4.2
Alloy 52 pin	1.0	--	10

The seal assembly was placed in a custom fixture mounted on the build plate in the Renishaw AM250. The fixture centered the part to the laser and the laser was focused 2 mm below the top surface of the glass preform. The custom fixture heated the seal assembly to 170ºC under an argon atmosphere (< 2000 ppm O_2). The Nd:YAG laser was scanned across the glass on a point-by-point basis, spacing the points by 50 µm dwelling for 100 µs. The laser was initially scanned horizontally across the glass preform, rotated 60º and rastered again, then rotated 60º once more and rastered a third time, Figure 3. This raster sequence was repeated three times, scanning over the glass a total of nine times, taking approximately six seconds to complete. Table 3 summarizes the laser parameters used to form the seals.

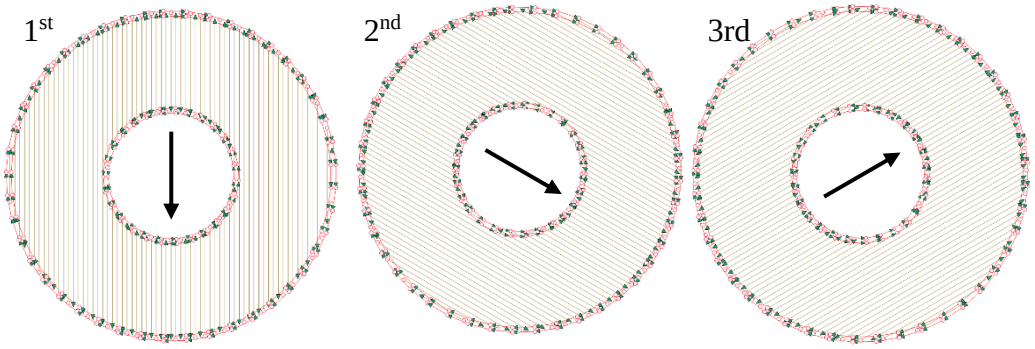

Figure 3: Raster path took by the SLM scanning horizontally, rotating the horizontal raster 60^{o} between each step. Arrow indicates direction of the laser scanning.

Table 3: Laser sealing parameters for LAM processed seals.

Laser Power (W)	Exposure Time (μs)	Hatch Spacing (μm)	Point Distance (μm)	Beam Width (μm)
162	100	85	50	50

2.3. CONVENTIONAL SEALING METHOD

Seals were produced using a conventional furnace sealing method with the same components described in Table 2. The assembled seals were placed in a tube furnace (Thermal Technology LLC, Minden, NV) under flowing argon. A graphite spacer was placed underneath the glass preform to hold the glass in place. The sealing schedule for the furnace is shown in Table 4. The total time for this sealing cycle was two and a half hours.

Table 4: Furnace schedule for the conventional furnace sealing process.

Step	Ramp Rate (°C/min)	Set Temperature (°C)	Hold time (Min)
1	20	980	12
2	-30	460	-
3	-5	100	-

2.4. LEAK TESTING

Helium leak rate testing was done with a Varian 979 (Agilent Technologies, Santa Clara, Ca) to characterize the hermeticity of the sealed parts. A custom fixture, shown in Figure A.1, was used to test the samples. Helium leak rate values for the seals, averages in Table A.1, were compared to an Al plug. If the leak rates were within an order of magnitude of 1.2 of the Al plug, the seals were considered hermetic. Further description in the Appendix.

2.5. ANALYTICAL SCANNING ELECTRON MICROSCOPY

Single pin seals produced by both methods were mounted in epoxy (VariDur, Buehler, Lake Bluff, Il), then cut down the pin axis using a diamond slow speed saw. These cross-sections were then polished using silicon carbide polishing pads and a diamond slurry to a 1μm finish.

The polished cross-sections were then coated with a thin layer of carbon. The sputter coater (Denton, Moorestown, NJ) was set to 60 mA and operated for 9 seconds. Secondary electron images of the samples were captured by a Helios 5 Hydra dual beam scanning electron microscope (SEM) (Thermo Fisher Scientific, Waltham, MA) with a

10 keV, 0.2 nA electron beam. Energy dispersive spectroscopy (EDS) was done using 20keV beam with a UltraDry detector (ThermoScientific, Waltham, MA). Line scans were performed across the glass-shell interface, with x-ray intensities measured for 5 seconds each at about 15 points in the metal and 35 points in the glass. The x-ray intensities were converted to elemental concentrations (atom %).

3. RESULTS AND DISCUSSION

3.1. OPTICAL AND THERMAL PROPERTIES OF THE DOPED SEALING GLASSES

Figure 4 shows the normalized absorption spectra collected from the copper-doped (blue lines) and iron-doped (red lines) glasses. The spectra were normalized to sample thickness (d) and by subtracting the spectrum of an undoped glass. The shaded areas on the graph indicate the maximum and minimum values recorded from at least three glasses doped with the same nominal metal oxide contents.

The iron-doped glasses have a maximum absorbance near the Nd:YAG wavelength at 1064 nm, but absorbance varied sample-to-sample. This variance may be due to the batch and melt histories of the different samples which control the redox reaction between tin and iron (Equation 2). The CuO-doped glasses have lower, but more reproducible, absorbance values at 1064 nm.

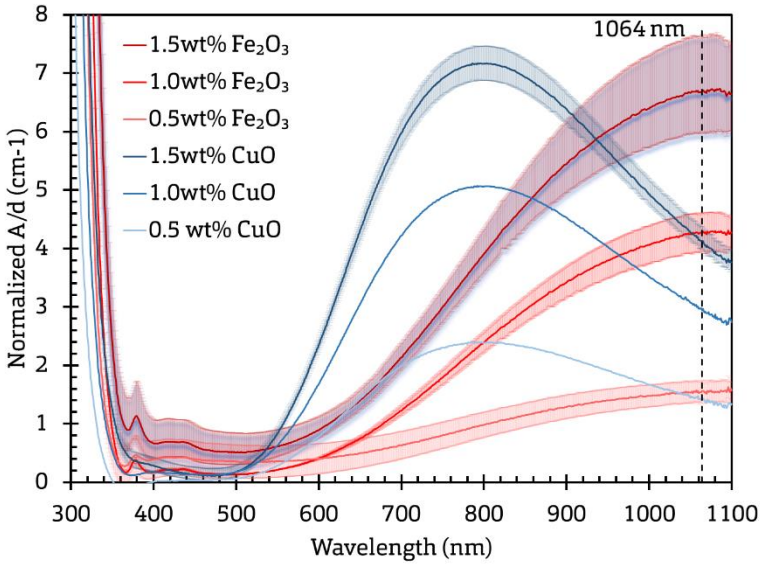

Figure 4: Normalized UV-Vis absorption spectra of Fe_2O_3 (red) and CuO (blue) doped Gl-1860 glasses. The lines represent the average absorbance values and the bands outline the respective minimum and maximum values. The vertical line at 1064 nm is the wavelength of the Nd:YAG laser.

The absorbance values (A/d) at 1064 nm of the CuO- and Fe_2O_3-doped glasses are plotted in Figure 5 as functions of the weight fractions of the respective oxides per unit volume (cm^3). Those concentrations (c) were calculated from the batched compositions and the glass densities (ρ), according to Equation 4. The extinction coefficient, δ (cm^2/g-oxide) for each of the dopant oxides at 1064 nm was calculated from the Beer-Lambert law, Equation 5,[17] and determined to be 1.67±0.07 cm^2/g and 1.01 ±0.01 cm^2/g for Fe_2O_3 and CuO dopants, respectively.

$$c = \frac{wt\ oxide}{wt\ glass} \cdot \rho \tag{4}$$

$$A = \delta \cdot c \cdot d \tag{5}$$

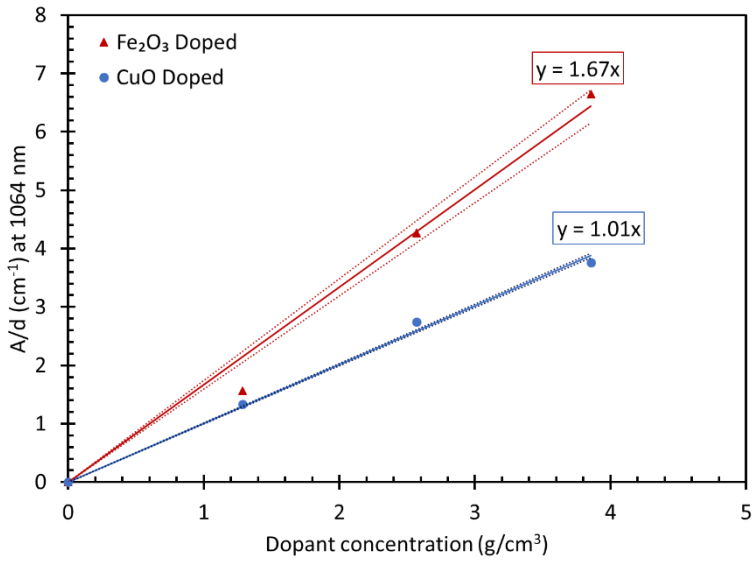

Figure 5 Beer-Lambert analyses of the Fe_2O_3 and CuO doped glasses for absorption at 1064 nm. Dashed lines are the 95% confidence interval and the linear slope is the extinction coefficient of the respective oxide.

Table 5 summarizes the thermal properties of the base glass and the glasses doped with 1.5 wt% Fe_2O_3 or CuO. The dopant increased the T_g of the glass, with Fe_2O_3 having a larger effect than CuO. Fe_2O_3 appeared to lower the CTE while not changing the T_{dil}. CuO had the opposite effect with T_{dil} lowered when compared to the undoped samples and CTE remaining within standard deviation.

Table 5: Thermal properties of the Gl-1860 base glass and glasses doped with 1.5 wt% Fe_2O_3 and CuO.

Glass	CTE (10^{-7}/°C)	T_g (°C)	T_{dil} (°C)
Gl-1860	108±9	460±4	559±3.00
1.5 wt% Fe_2O_3	95.5±0.7	480±1	558±6
1.5 wt% CuO	101±3.6	470±5	543±1

3.2. SEALS PRODUCED BY THE LAM PROCESS

Examples of a single-pin seal made with an iron-doped glass and a solid plug seal made with a copper-doped glass, both fabricated by the LAM process, are shown in Figure 6. The photographs of the top surfaces of the respective seals, Figures 6a-b, show that in each case, the glass filled the interior diameter of the metal shell. A ring of melted metal, indicated by the white arrows in each figure, is apparent on the shell surface around the seal. The laser raster pattern (Figure 3) extended over the shell surface by 400±110 μm and was intended to ensure complete heating of glass at the glass-shell interface. Bubbles are apparent in the respective bodies of each glass, and a copper-colored ring is apparent at the shell-glass interface of the sample sealed with the CuO-doped glass (Figure 6b).

The cross-sections of the seals, Figures 6c-d, show tight interfaces between the glass and shell (and glass and pin, for the iron-doped pin seal) extending several millimeters below the top surface of each glass, and then some separation of the glass and shell, indicated by the white circle on Figure 6c. The laser appears to have only melted the glass to a certain depth with the remain bottom half being unaffected from the processing conditions.

The shell-glass separation depth is 1.5±0.4 mm from the top surface of the glass for 1.5 wt% Fe_2O_3-doped seals and 1.4±0.6 mm from the top surface of the glass for the 1.5 wt% CuO-doped seals, two cross-sectioned seals of each dopant were used for the measurements. For the latter samples, the depth of the copper-colored layer was 0.5±0.2 mm (Figure 6d), These depths are less than the focal point of the processing laser, which was 2 mm below the initial glass surface.

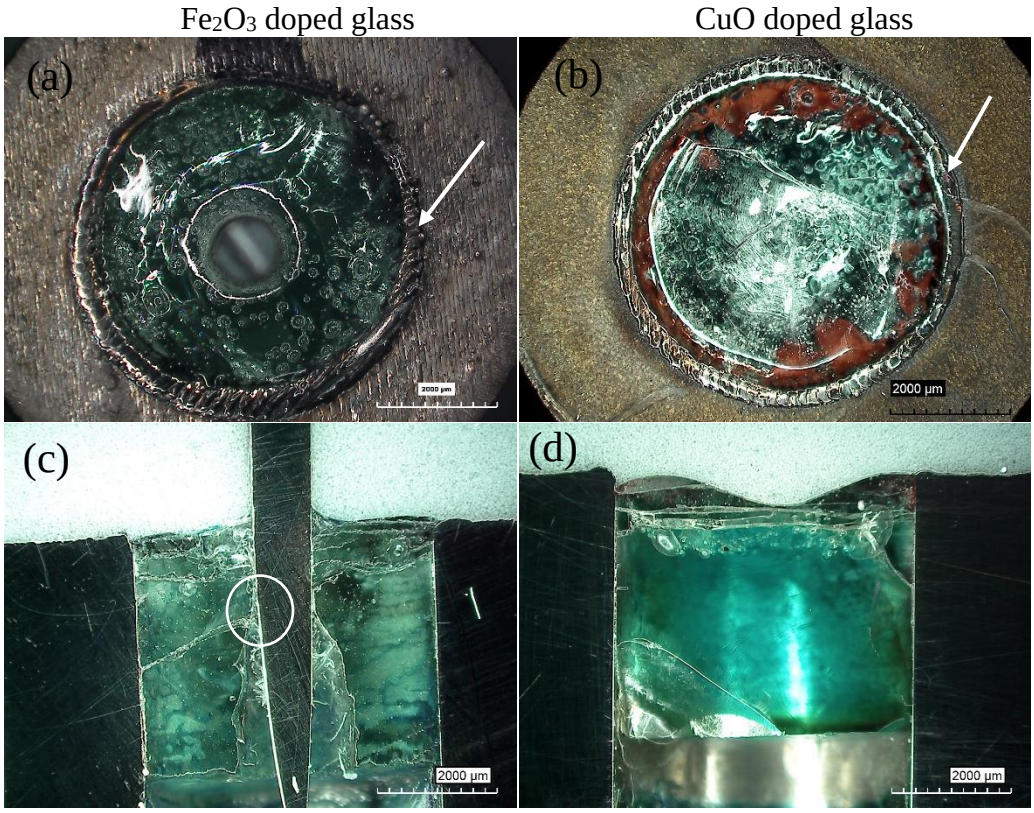

Figure 6: Top views, (a) and (b), and cross-sectional views, (c) and (d), of a LAM-processed pin seal made with an iron-doped glass (left) and a plug seal made with a copper-doped glass (right). The white circle indicates separation of a glass-metal interface. During the LAM process, the laser was rastered over the surface shown and those surfaces are at the top of the cross-sections.

Cracks are also apparent in the images of the two seals in Figure 6, particularly in the respective cross-sections. The release of this compressive stress when the sample was cross-sectioned could have produced the cracks shown in Figures 6c-d.

Table 6 summarizes the helium leak testing information collected on various pin and plug seals. Here, a sealed component was considered “hermetic” if it had a helium leak rate below 1.2 orders of magnitude higher than the Al plug. This value was chosen to account for the variability in the baseline helium leak rate measurements made with the aluminum plug.

Table 6: Pin and plug seal samples that passed the helium leak rate hermeticity test.

Glass Dopant	Pin Seals (LAM)	Plug Seals (LAM)	Pin Seals (Conventional)
1.5 wt% Fe_2O_3	8/40 (20%)	--	1/4 (25%)
1.0 wt% Fe_2O_3	0/12 (0%)	--	--
0.5 wt% Fe_2O_3	--	0/6 (0%)	--
Undoped	0/9 (0%)	--	--
1.5 wt% CuO	--	6/6 (100%)	1/4 (25%)
1.0 wt% CuO	--	4/6 (67%)	--
0.5 wt% CuO	--	0/6 (0%)	--

Table 6 shows that the fraction of LAM seals that were hermetic increased with increasing dopant levels for both the Fe_2O_3- and the CuO-doped glasses, and plug seals made with the latter glasses were most likely to be hermetic.

The CuO doped glass appears to have a higher success rate than the Fe_2O_3, though less samples were tested. The CuO reacting with the metal shell can create a very sturdy chemical bond at the glass-metal interface.[18] Additionally, the higher success rate in the larger doped glasses, of both dopants, could be from the oxide dopant aiding in chemical reactions for glass-metal adhesion.[1]

3.3. SEALS PRODUCED BY THE CONVENTIONAL FURNACE PROCESS

Figure 7 shows images collected from representative samples of seals made using the conventional furnace process. Of particular note is the poor wetting of both the iron-

doped and copper-doped glasses to the 304L shell. In general, better wetting was observed to the Alloy-52 pin. The poor wetting to the shell and not the pin may be due to the surface roughness of the shell.[19] To improve the wettability of the glass to the shell and initial oxide layer could be introduced on the metal shell before sealing.[1]

Where the glasses were in contact with the shells and pins, there appears to be good bonding, without the gaps noted at the bottoms of the glass-shell interfaces for the LAM seals (Figures 6c,d). Figure 7b shows that the top of a copper-doped seal has turned a copper-color, and the cross-section of a CuO-doped sample (Figure 7d) shows that this discoloration extends along the entire glass-shell interface and is evident on the exposed Alloy-52 pin.

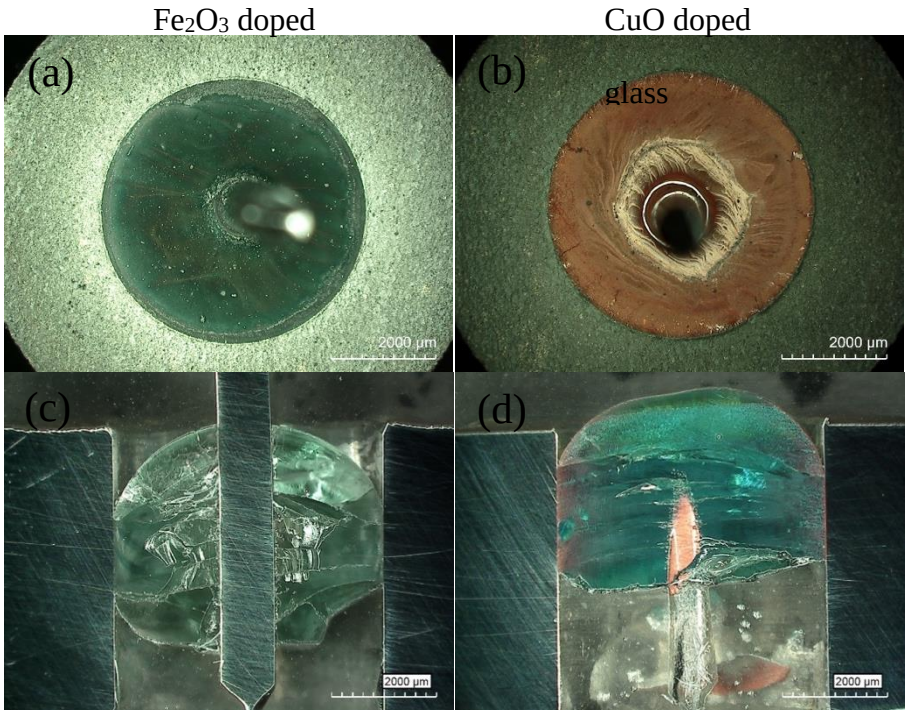

Figure 7: Top view, (a) and (b), and cross-sectional view, (c) and (d) of seals produced using the LAM sealing method. Images (a) and (c) are seals made with Fe_2O_3 doped glass. Images (b) and (d) are seals made with CuO doped glass.

3.4. SEM/EDS ANALYSIS

The cross-sectioned samples of LAM and conventional GtM seals were further analyzed by analytical scanning electron microscopy. For each sample, a spot at the interface between the shell and the sealing glass, approximately 500 nm below the top surface of the glass, was analyzed. Figure 8 shows representative SEM images of the interfaces that formed between the Fe_2O_3-doped (1.5 wt%) glass and the shell processed by the conventional furnace method (a) and the LAM process (c), and the interfaces that formed between the CuO-doped (1.5 wt%) glass and the shell processed by the conventional furnace method (b) and the LAM process (d).

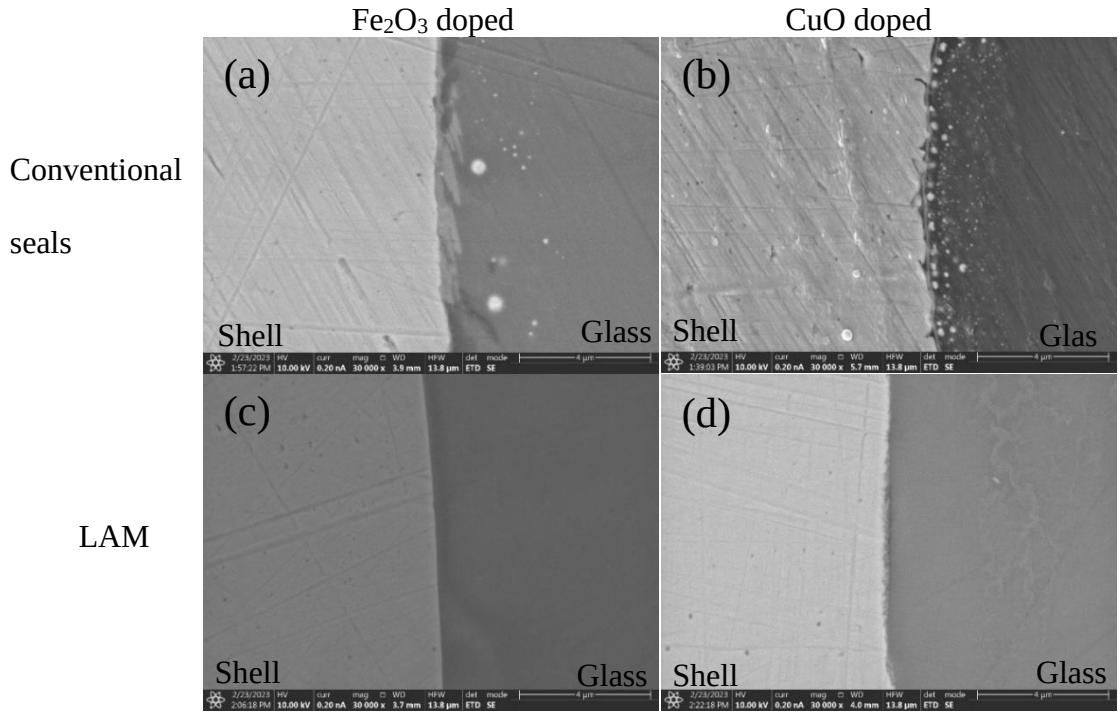

Figure 8: SEM images of the shell-glass interfaces of a (a) conventionally processed and (b) LAM processed 1.5 wt% Fe_2O_3-doped glass seals, and (c) conventionally processed and (d) LAM processed 1.5 wt% CuO-doped glass seals.

The interfaces of both conventionally processed seals have much more heterogeneous microstructures than do the interfaces of the LAM-processed seals. The

heterogeneities include plate-like phases, about 0.7 μm thick, at the interface with the Fe_2O_3-doped glass and bright, sub-micron spheres extending several microns from the interfaces with both glasses. The CuO-doped glass similarly has the bright sub-micron spheres.

Compositional information was obtained from EDS line scans collected across each interface. Figure 9 shows the Fe and Cr profiles across the interfaces between the 304L stainless steel shell and the Fe_2O_3-doped glass for seals made by the conventional process and by the LAM process. The horizontal lines shown in the respective SEM images indicate where the EDS line scan data were collected. There is some depletion of both Fe and Cr from the outermost 1 micron of the metal side of both interfaces appear to have diffused several microns into the glass. The expanded EDS profiles shown in the inset to Figure 9 indicate that the plate like features seen in the SEM image of the conventional seal are enriched in Cr.

Figure 10 shows O, Na, and Sn EDS line scans across the same stainless steel/Fe2O3-doped glass interfaces. There appear to be higher concentration of O in the vicinity of the plate like features at the interface of the conventional seal compared to the interface of the LAM processed seal. In addition, the inset to the EDS scans in Figure 10 indicates that the bright particle seen in the corresponding SEM image of the conventional seal is rich in Sn, as well as Fe (Fig. 9).

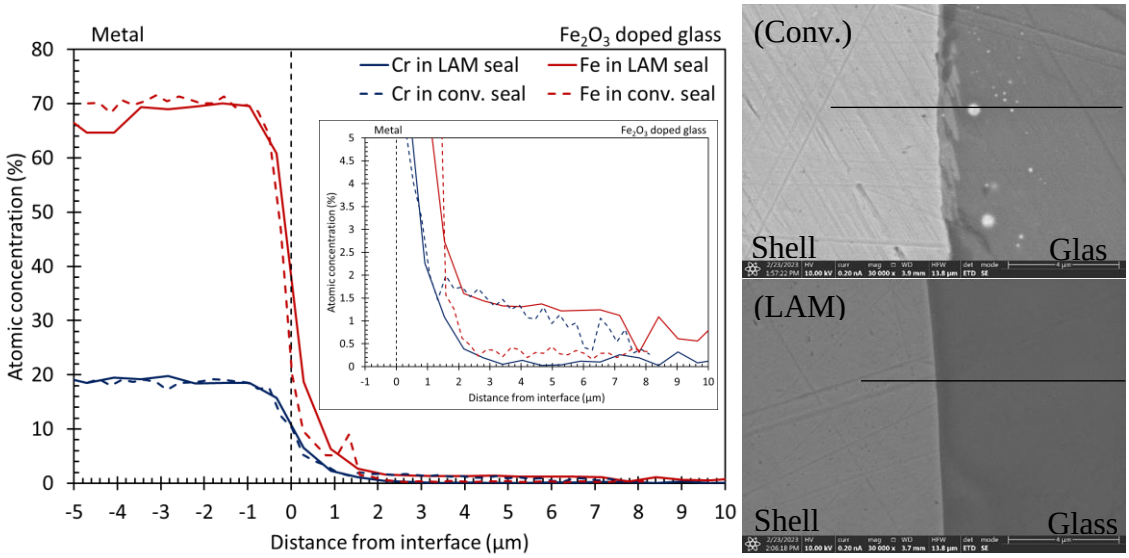

Figure 9: EDS line scans for Cr and Fe across the interfaces of conventional and LAM seals made with Fe_2O_3-doped glasses. The horizontal lines in the SEM images to the right trace the respective paths of EDS line scans.

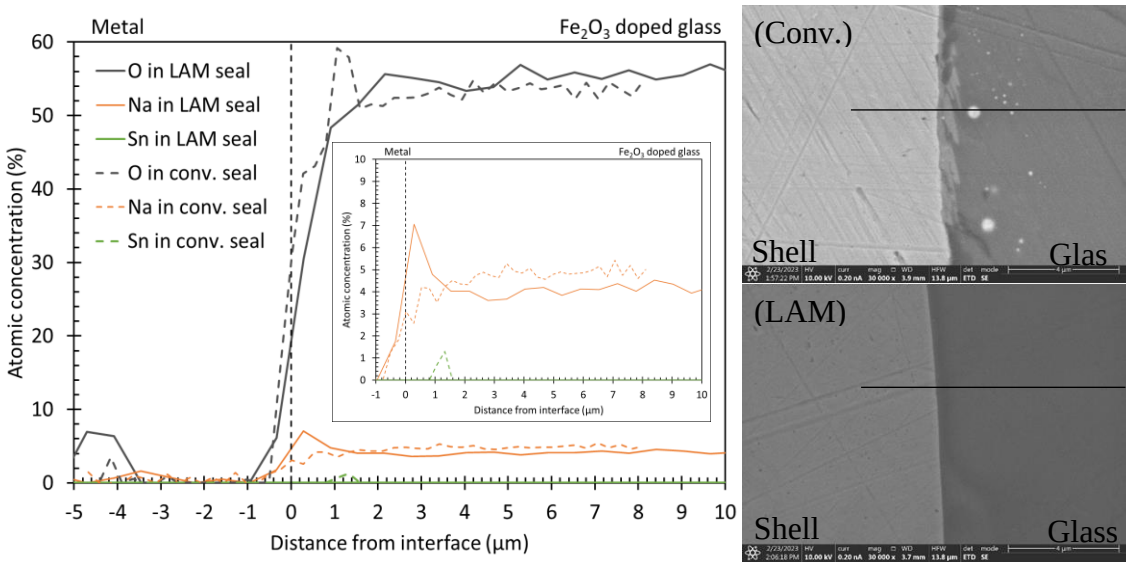

Figure 10: EDS line scans for O, Na, and Sn across the interfaces of conventional and LAM seals made with Fe_2O_3-doped glasses. The horizontal lines in the SEM images to the right trace the respective paths of EDS line scans.

Figures 11 and 12 show the EDS compositional profiles across the interfaces of the conventional and LAM-processed seals made with glasses doped with 1.5 wt% CuO.

The Fe and Cr profiles indicate greater diffusion of Fe and Cr into the furnace sealed glass, but a build-up of both elements about 3 microns from the interface of the LAM processed seal. Figure 12 shows that there also is a build-up of Cu, and perhaps a deficit of O, at this same distance from the interface. These elements appear to be associated with the light-colored particles evident in SEM image of the LAM-processed seal. This correlates with the reduced copper in the optical images, Figure 3.4d. There is less build-up of sodium at the interface of the LAM-processed seal made with the CuO-doped glass (Figure 12) as there was with the LAM-processed seal made with the Fe_2O_3-doped glass (Figure 10).

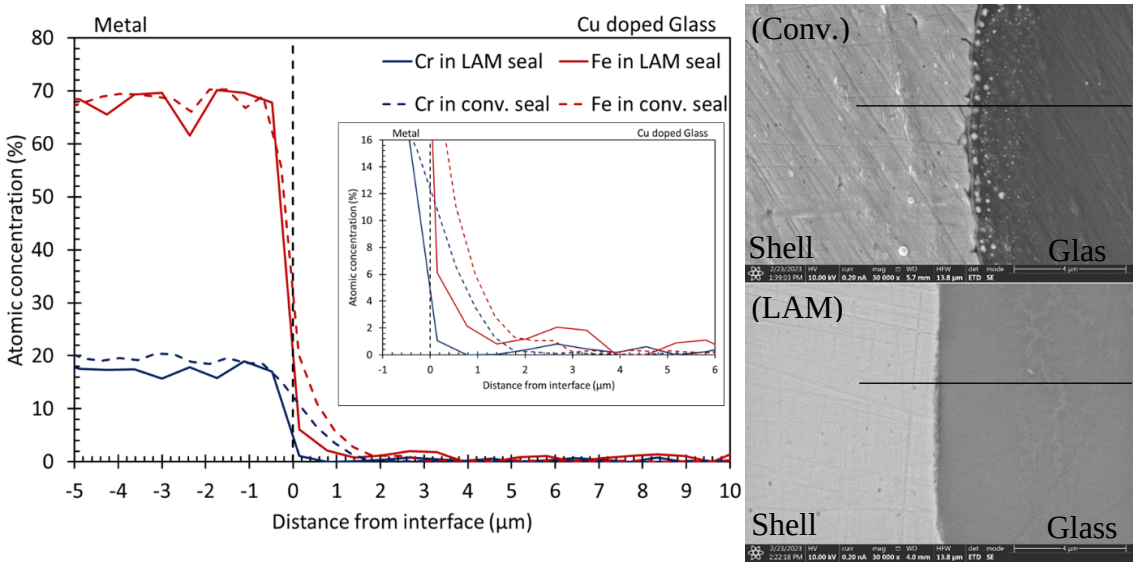

Figure 11: EDS line scans for Cr and Fe across the interfaces of conventional and LAM seals made with CuO-doped glasses. The horizontal lines in the SEM images to the right trace the respective paths of EDS line scans.

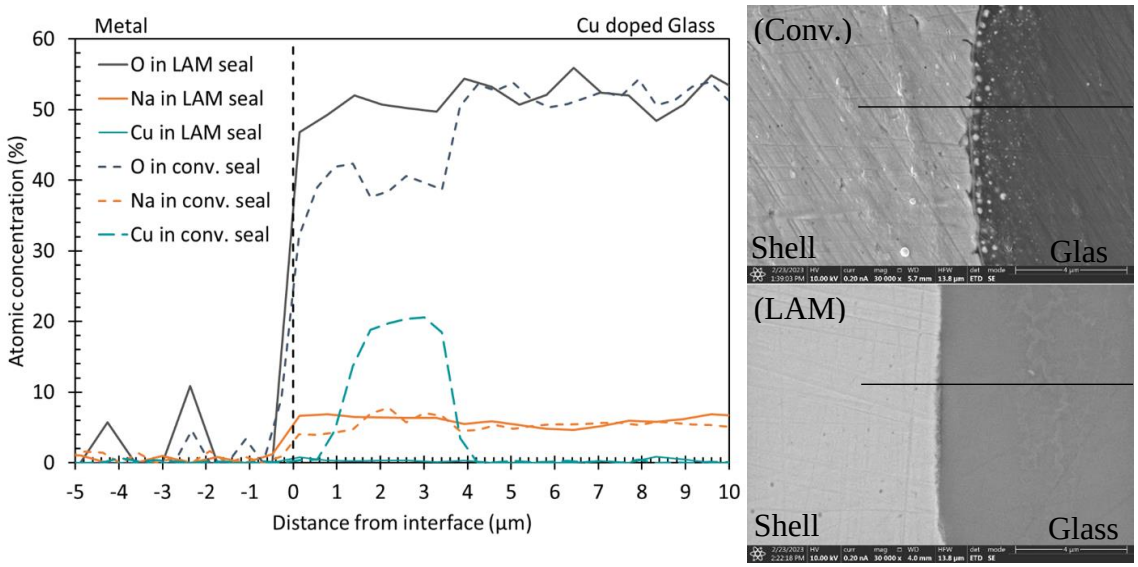

Figure 12: EDS line scans for O, Na, and Cu across the interfaces of conventional and LAM seals made with Fe_2O_3-doped glasses. The horizontal lines in the SEM images to the right trace the respective paths of EDS line scans.

The development of the microstructural features seen in the optical images and SEM/EDS analyses can be understood by considering possible redox reactions between components of the respective glasses and metals, Equations 6-13. Those reactions were modeled using the databases[20] associated with Factsage v8.2 (Thermfact/CRCT (Montreal, Canada) and GTT-Technologies (Aachen, Germany)), assuming an argon atmosphere (1 atm) with 2000 ppm O_2. The free energies of the following reactions that may be occurring at the interfaces with the Fe_2O_3-doped glasses were calculated at 980°C, the furnace temperature used for the conventional seals.

$$Fe + Na_2O \rightarrow FeO + 2Na_g \qquad \Delta G = -82.4\ kJ/mol \tag{6}$$

$$Cr + \frac{3}{2}Na_2O \rightarrow \frac{1}{2}Cr_2O_3 + 3Na_g \qquad \Delta G = -121\ kJ/mol \tag{7}$$

$$Fe + Fe_2O_3 \rightarrow 3FeO \qquad \Delta G = -82.3\ kJ/mol \tag{8}$$

$$Cr + \frac{3}{2}Fe_2O_3 \rightarrow \frac{1}{2}Cr_2O_3 + 3FeO \quad \Delta G = -204\ kJ/mol \tag{9}$$

$$Fe + \frac{1}{2}SnO_2 \rightarrow FeO + \frac{1}{2}Sn \qquad \Delta G = -64.2\ kJ/mol \tag{10}$$

$$Cr + \frac{3}{4}SnO_2 \rightarrow \frac{1}{2}Cr_2O_3 + \frac{3}{4}Sn \qquad \Delta G = -174\ kJ/mol \tag{11}$$

The Na_2O reduction reactions become increasingly more favorable in lower partial pressures of Na_g, reducing atmospheres.[7] The Cr reactions are more favorable than the Fe reactions, lower ΔG^o.

There is a large concentration of Cu that correlates with a decrease in O concentration, 1-4 μm deep into the glass. This would support the reduced Cu found in the optical image, Figure 7d, with the bright spheres in Figure 8b being copper metal. Possible reduction reactions are listed, Equations 12-13.

$$Fe + CuO \rightarrow FeO + Cu \qquad \Delta G = -66.1\ kJ/mol \tag{12}$$

$$Cr + \frac{3}{2}CuO \rightarrow \frac{1}{2}Cr_2O_3 + \frac{3}{2}Cu \qquad \Delta G = -97.4\ kJ/mol \tag{13}$$

The EDS profiles show that Cr and Fe diffused more deeply into both the Fe_2O_3- and CuO-doped glasses fabricated in the furnace than by the LAM process. This might be related to the longer times that the furnace processed glasses were heated at temperatures where diffusion is significant[9] and these longer times may allow more SnO and CuO to reduce at the furnace-processed interfaces, creating the sub-micron particles that are evident in the respective SEM images. The shorter process times and the resulting "cleaner" glass-metal interfaces may prove advantageous for LAM processing of glass-metal seals, particularly when reactive metals are involved.

4. SUMMARY

Hermetic glass-to-metal seals were produced using a laser assisted manufacturing (LAM) process and a conventional furnace process. Fe_2O_3, co-doped with SnO, and CuO dopants were added to a commercial silicate sealing glass to increase at the near infrared wavelength of the Nd:YAG laser used in the LAM process. The glasses were sealed with stainless steel shells and with or without Alloy-52 pins. LAM seals glasses doped with 1.5 wt% of either dopant had the best hermeticity results, based on helium leak testing. The cross-sectional interfaces of LAM seals showed fewer heterogeneities than what were found for the furnace-processed seals and this could be explained by the shorter processing times of the former method.

REFERENCES

1. Donald I. *Glass-to-metal seals*. Soc. Glass Technol. (2009)
2. Rulon, R. *Introduction to Glass Science*. Plenum Press. p. 661–704. (1972)
3. Tomsia A., Pask J., Loehman R. *Engineering material handbook, Vol. 4, Ceramic and glasses.* ASM international. :493. (1991)
4. Partridge G. *Glass-to-metal seals*. Soc. Glass Technol. (1949)
5. King B., Tripp H., Duckworth W. *J Amer. Ceram. Soc*. 42(11):504. (1959)
6. Pask J. *Proc. Porcelain Enamel Inst. Tech*. forum. 33:1 (1971)
7. Brennan J., Pask J. *J. Amer. Ceram. Soc.* 56(2): 58. (1973)
8. Tomsia A., Pask. *Dent Mater.* 2:10 (1986)
9. Tomsia A., Feipeng Z., Pask J. *J Amer. Ceram. Soc.* 68(1):20. (1985)

10. Donald I., Mallinson P., Metcalfe B., Gerrard L., Fernie. *J. Mater. Sci*. 46:1975. (2011)

11. Luo J., Pan H., Kinzel. *J. Manufacturing Sci. Eng.* 136(6): 061024. (2014)

12. Montenero A, Friggeri M, Giori D C, Belkhiria N, Pye L D. *J. of Non-Crystalline Solids* 84: 45. (1986)

13. Kutub AA. *J. Mater. Sci*. 23(7):2495. (1988)

14. Hayashi Y, Matsumoto K, Kudo M. *J. of Non-Crystalline Solids*. 282(2):188. (2001)

15. Wongsing T, Kaewkhao J, Limsuwan P, Kedkaew C. *Procedia Engineering*. 32:807 (2012)

16. ASTM C693-93, "Standard Test Method for Density of Glass by Buoyancy", ASTM International, West Conshohocken, PA. (2019)

17. Singh SP, Kumar A. *J. Mater. Sci*. 30(11):2999. (1995)

18. Donald I., Metcalfe B., Gerrard L., *J Amer. Ceram. Soc.* 91(3):715. (2008)

19. Marshall SJ, Bayne SC, Baier R, Tomsia AP, Marshall GW. *Dental Materials*. 26(2):11. (2010)

20. C. W. Bale E., Bélisle P., Chartrand S. A. et.al. FactSage Thermochemical Software and Databases. Calphad. 54: 35. (2016)

SECTION

3. CONCLUSION

The objective of this research was to product glass-to-metal (GtM) seals using additive manufacturing techniques.

Selective laser sintering (SLM) and Digital light processing (DLP) methods were utilized to produce the 304L stainless steel shell and silicate sealing glass preform components, respectively. The sealing glass powder was mixed with a photosensitive resin in a 2:1 weight ratio for the purpose of DLP printing. The printed preforms underwent an organic removal (burnout) and sintering schedule to produce dense glass preforms with a 0.97 relative density.

The burnout schedule was determined through a mixture of thermal gravitational analysis (TGA), differential scanning calorimetry (DSC), and a series of screening experiments. The hold temperatures were determined to be 285^{o}C and 500^{o}C in endothermic regions of the DSC, correlating with mass loss data in the TGA. Ramp rate and hold times were found with the screening experiment with the goal of reducing defects seen in the sample with the chosen burnout schedule to be 0.25^{o}C/min to 285^{o}C, holding for 2 hours and a 1^{o}C/min ramp to 500^{o}C, holding for 5 hours.

Video experiments during isothermal holds were used to create a densification curve for the sintering glass preforms. Viscous sintering models were applied to the densification curves determining a fit viscosity for the glass. The model fit viscosity

values were about 0.75 of an order of magnitude higher from the measured viscosity values through thermal mechanical analysis (TMA)

Hermetic seals were produced from the printed shell and sintered preforms. After sealing the glass had many bubbles indicating not all the organics were effectively removed before the sealing process.

Hermetic seals were also produced used a laser assisted manufacturing (LAM) process. A Nd:YAG laser rastered over a solid glass preform, melting the glass allowing to bond to the SLM printed 304L shells and the Alloy 52 pin. Transition metal oxides, Fe_2O_3 or CuO, were added to the sealing glass to increase the absorption of the laser's wavelength, 1064 nm. Fe_2O_3 doped glasses were co-doped with SnO to reduce Fe^{3+} to Fe^{2+}, the near-IR absorbing valencene state, in the glass.

Cross-section of the LAM and conventionally made seal were analyzed with electron microscopy techniques finding the LAM seals had reduced interfacial morphologies. In the conventional seals these morphologies were found to be metallic oxides and metal spheres through energy dispersive spectroscopy (EDS). These heterogeneous microstructures formed through a series of redox reactions at the interface between Fe and Cr from the metal shell and oxides from the glass. These reactions were detected in the LAM produced seals, though to a lesser degree than their furnace processed counterparts.

4. FUTURE WORK

The following list are some issues found while conducting this research that should be considered for further studies.

1. With the bubbles formed in the printed preform seals, Figure 18 in Paper I, and the gap separation in the LAM seals, Figure 6c-d in Paper II, a non-destructive method should be utilized to measure the bubble size and where this gap occurs. MicroCT scans on the seals could provide this information without having to cross-section the samples.
2. The sintered preform in Paper I, Figure 15, had remaining organics and resulted in bubbles in the final seal produced. A more effective burnout schedule should be explored with the goal of a clear sintered preform.
3. Further studies should be conducted into the cause of difference of viscosities measured by TMA and calculated with the vicious sintering model.
4. The laser for the LAM sealing process should be focused near the bottom of the preform. This may result in a deeper laser penetration and a larger area of glass bonded to the metal shell/pin.
5. Ti metal shell have been found to react significantly with silicate glasses, forming a detrimental interfacial layer. With the reduction of processing time the LAM method offers, Ti and silicate glasses could be paired with a "cleaner" interfacial layer than previously studied sealing methods.
6. Different geometries of seals should be attempted with the SLM printed shells and DPL printed glass preforms.

APPENDIX

HELIUM LEAK RATE TESTING

Figure A.1 shows the custom fixture used to test seals on the Varian 979 leak detector. An overpressure of 2 psi of He was implemented on the seal, while a vacuum was pulled on the opposite. The leak rate value of the Al plug was $4.91 \pm 7.39 \times 10^{-8}$ atm-cc/sec. With such a large variance on the leak rate of the Al plug it was used a baseline for the seal leaks rates.

The "read standard leak" function of the machine was used unless when the vacuum was being pulled on the sample did not reach a pressure value less than 0.13 Pa, then the test was considered non-hermetic. The leak rate of the seal was noted when the value equilibrated after reaching a pressure of 50 Pa during the "read standard leak" test. Seals were considered hermetic when the leak rates, averages in Table A.1, were within 1.2 order of magnitude of the Al plug. As an example, if Al plug has a leak rate of 1.2×10^{-8} atm-cc/sec than any seal with a leak rate higher than 1.9×10^{-7} atm-cc/sec was not considered hermetic.

Figure A.1: Image of the custom fixture used to test seals hermiticity.

Table A.1: average leak rate values for the seals of each dopant level and the amount of the seals that passed the hermetic conditions.

Processing Method	Glass Preform	Leak rate (10^{-7} atm-cc/s)	% Hermetic by He leak testing
LAM Seals	1.5 wt% Fe_2O_3	2.0±0.3	8/40
	1.0 wt% Fe_2O_3	--	0/12
	0.5 wt% Fe_2O_3	3.7	0/6
	Undoped	17	0/9
	1.5 wt% CuO	2.6±0.3	6/6
	1.0 wt% CuO	2.9±0.3	4/6
	0.5 wt% CuO	--	0/6
Conventional Seals	1.5 wt% Fe_2O_3	4.6±0.9	1/4
	1.5 wt% CuO	1.2±0.9	1/4
	Printed preform	1.2±0.4	3/4

BIBLIOGRAPHY

1. Donlad I. *Glass-to-metal seals*. Soc. Glass Technol. (2009)
2. Rulon, R. *Introduction to Glass Science*. Plenum Press. p. 661–704. (1972)
3. Pask J. *Proc. Porcelain Enamel Inst*. Tech. forum. 33:1 (1971)
4. Partidge G. *Glass-to-metal seals*. Soc. Glass Technol. (1949)
5. King B., Tripp H., Duckworth W. *J Amer. Ceram. Soc*. 42(11):504. (1959)
6. Glass-to-Metal Seals and Feedthroughs. *Complete Hermetics*. n.d.
7. Rawson H. *Properties and application of glass*, Elsevier. (1980)
8. Mayer P., Topping J., et.al. *J. Can. Ceram. Soc*. 43:43(1974)
9. Donlad I., Mallinson P., Metcalfe B., Gerrard L., Fernie. *J. Mater. Sci*. 46:1975. (2011)
10. Brennan J., Pask J. *J. Amer. Ceram. Soc*. 56(2): 58. (1973)
11. Tomsai A., Pask. *Dent Mater*. 2:10 (1986)
12. Passerone A., Valbusa G., Biagini E., J. Mat. Sci. 12:2456, (1977)
13. Donald I., Metcalfe B., Gerrard L., *J Amer. Ceram. Soc*. 91(3):715. (2008)
14. Brow R., Watkins., *Technology of Glass, Ceramic, or Glass-Ceramic to Metal Sealing*. Am. Soc. Mech. Eng. pp 25. (1987)
15. Medhe S. *Chemical and Biomolecular Engineering*. 3(4):51. (2018)
16. Singh S., Ramakrishna S., Singh R. *Journal of Manufacturing Processes*. 25:185. (2017)
17. Kruth JP., et. al. *J. Mat. Proc. Tech*. 149(1):616. (2004)
18. Das S. *Advanced Engineering Materials*. 5(10): 701. (2003)
19. Zhang H., Xu M., Kumar P., Li C., Liu Z., Zhang Y. *Journal of Materials Processing Technology*. 297:117279. (2021)

20. Sufiiarov, V., et al. *Procedia Engineering*. 174(Jan): 126. (2017)

21. Luo J., Pan H., Kinzel. *J. Manufacturing Sci. Eng.* 136(6): 061024. (2014)

22. Datsiou KC, Saleh E, Spirrett F, et.al. *J. Am. Ceram. Soc*. 102(8):4410. (2019)

23. Shelby J. *Introduction to Glass Science and Technology*. Royal Soc. Chem. (2005)

24. Varshneya A., Mauro J. *Fundamentals of Inorganic Glasses*. Elsevier. (2019)

25. Montenero A, Friggeri M, Giori D C, Belkhiria N, Pye L D. *J. of Non-Crystalline Solids* 84: 45. (1986)

26. Kutub AA. *J Mater Sci*. 23(7):2495. (1988)

27. Gibson I., Rosen D., Stucker B. *Additive Manufacturing Technologies*. Springer. (2012)

28. Bae S., Kinb B. *Appl. Sci.* 11:6835 (2021)

29. Baumgartner S., Gmeiner R., Schönherr JA., Stampfl J. *Materials Science and Engineering: C*. 116:111180. (2020)A

30. Liu Z, Pan W, Wang K, et al. *Advanced Materials*. 34(7):2106183(2022)

31. Hermanson L. *Engineering material handbook, Vol. 4, Ceramic and glasses.* ASM international. :135. (1991)

32. Zhang J., Edirisinghe M., Evan J. *Mater. Lett.* 7:15 (1988)

33. Lonkar, N. R., R. O. Loutfy, and C. V. Cox. "Process for Removing Carbon or Carbon Compounds Comprised in Binders From Non-Oxide Ceramics, and Sintered Bodies Obtained Therefrom." *Patent NumberEP 0276148* (1988)

34. Strangle G., RheeD., Aksay I. *Proceedings of ANTEC89, Society of Plastics*. :1066 (1989)

35. R. Gilissen and A. Smolders. *High Tech*. Ceramics. p567. (1987)

36. Rahman M. *Sintering of Ceramics*. CRC press. (2008)

37. German, R. M. *ASM International, Engineered Materials Handbook., 4*: 260.(1991)

38. Frenkel J. *Phys*. 9[S]:385. (1945)

39. Mackenzie J., Shuttleworth R. *Proc. Phys. Soc.* 62:833. (1949)

40. Scherer G. *J. Am. Ceram. Soc.* 60:236. (1977)

41. Prado M, Zanotto E, Müller R. *J. of Non-Crystalline Solids*. 279(2):169. (2001)

VITA

Aaron Reece Read, son of Ted and Diane Read, was born in Wurzburg, Germany. Traveling with his family they finally settled in Rolla, MO in the summer 2012.

Aaron graduated with his high school diploma from Rolla High School in May of 2016. August 2016, he enrolled at Missouri University of Science and Technology pursuing a Ceramic Engineering degree. During his time as an undergraduate, Aaron became a member of the Keramos chapter, Material Advantage, and the Gaffer's Guild on campus. He spent his summers working with a co-op with Kohler Co., 2018, and an internship with ZAF energy systems, 2020, the remaining summers he spent in the Materials Research Center (MRC) at Missouri S&T working for various research projects. Aaron was awarded his B.S. for Ceramic Engineering in December 2020.

In January 2021 he joined Dr. Brow's group at Missouri S&T to pursue his M.S. in Materials Science and Engineering. His work focused on the production of glass-to-metal seals using additive manufacturing techniques funded by Kansas City National Security Campus (KCNSC). Summer 2022 he took an internship with KCNSC to continue his research at their facility. Aaron received his M.S. in Materials Science and Engineering in May 2023 form Missouri University of Science and Technology.